This Paper is a working manuscript, under preparation for submission to a peer reviewed journal

Ladakh's Rock Varnish: A potential Geomaterial for astrobiological studies

Amritpal Singh Chaddha[*a, b], Anupam Sharma[*a], Narendra Kumar Singh[b], Sheikh Nawaz Ali[a], P.K. Das[a], S.K. Pandey[a], Binita Phartiyal[a], Subodh Kumar[a]

[a]Birbal Sahni Institute of Palaeosciences, 53 University Road, Lucknow-226007, India

[b]Department of Chemistry, Faculty of Science, University of Lucknow, Lucknow-226007, India

Corresponding Author:

[*]E-mail: anupam110367@gmail.com; amrit.chemsingh@gmail.com

Graphical Abstract

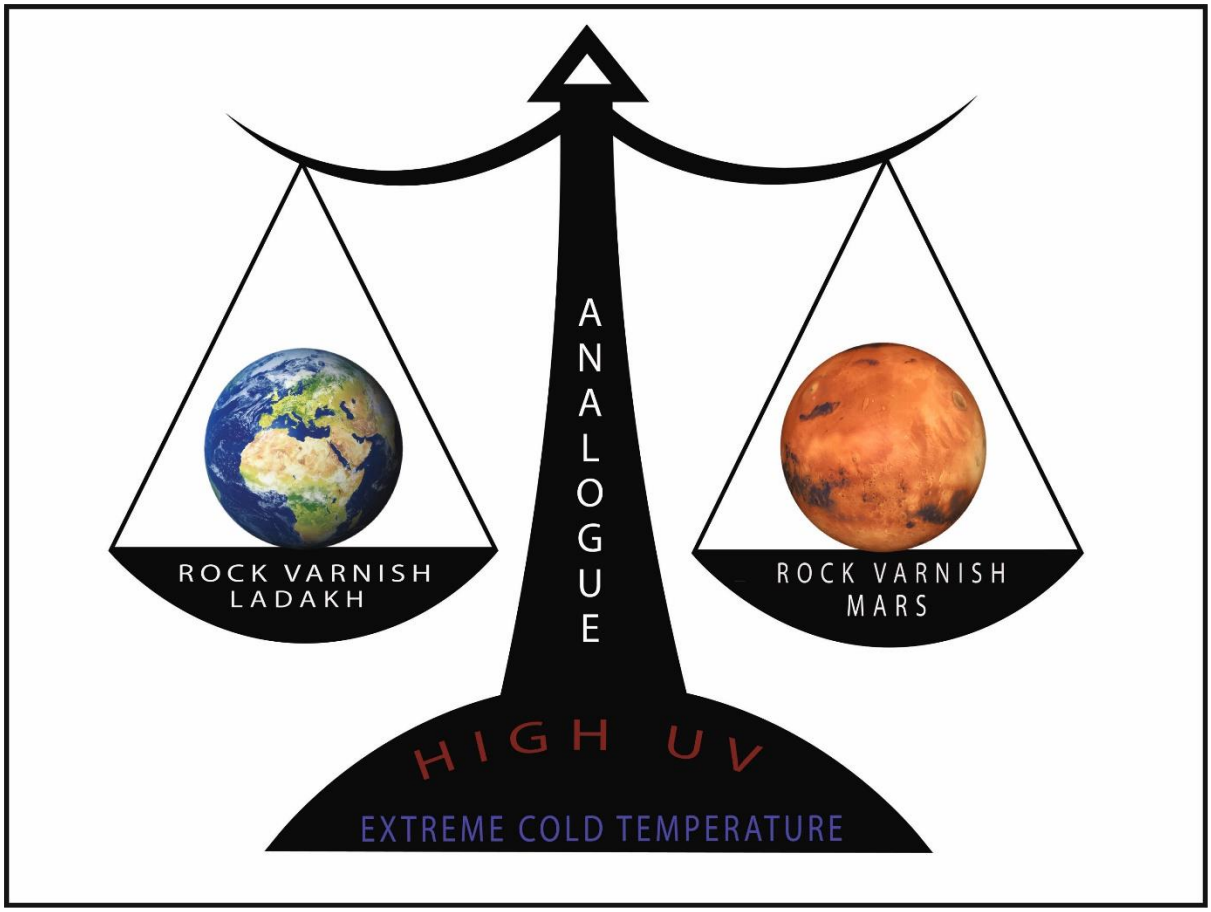

Abstract

Rock varnish, a dark-coloured natural feature rich in manganese (Mn), iron (Fe), and clay minerals, is believed to provide nutritional support to microbiota. Thus, rock varnish is considered a unique substrate for potential microbial life to thrive in the extreme environments on Earth that are comparable to their planetary analogues. However, little is known about the occurrence of microbiota in rock varnish, as the microbes found on the varnish are quite diversified. We present here the new morphological and chemical results of microbial forms found in rock varnish samples from Ladakh, a potential site for hosting life in extreme environments. Our results demonstrate the presence of putative magnetofossils type biological entities in the form of nanochains present in the rock varnish layer that coincide with high magnetic susceptibility values of varnish samples. Further, the higher concentrations of oxidised fractions of Mn^{4+}, and carboxylic acid functionality on the varnish surface revealed the signatures of organic entities. These collective results point towards the enriched concentration of magnetic minerals on the varnish layer that are possibly sourced through biotic forms. Consequently, the rock varnish can serve as a "black box" of ancient environmental records, as well as a potential geomaterial for astrobiological studies from the Martian analogue field location of Ladakh, which needs to be explored further for extensive biogeochemical studies.

Keywords

Rock varnish, Mars-analogue, Extreme environment, Astrobiology, Ladakh, Magnetotactic bacteria, X-ray photoelectron spectroscopy, Magnetic minerology

Introduction

Rock varnishes are thin, dark-brown to black coatings of manganese and iron oxides on the surface of rocks held together by clay minerals and found in arid to semi-arid regions worldwide (Chaddha et al., 2021b; Dorn and Oberlander, 1981; Potter and Rossman, 1977). Although abiotic and microbiological activities are thought to be important for its formation, the mechanism underlying the selective deposition of iron and manganese within the clay matrix remains unknown. As a result, the origins of this veneer are still a mystery (Kuhlman et al., 2006; Potter and Rossman, 1979). These micro coatings on rocks have recently sparked researchers' interest in investigating terrestrial geomicrobiology and its relationship to rock

weathering processes, which is a useful tool in developing models for similar processes that may have occurred on Mars (Krinsley et al., 2009). Since the 1976 Viking landers captured images of lustrous black coats (Herkenhoff et al., 2008), it has been speculated that rock varnish on Mars, similar to rock varnish coatings on Earth, could hold the key to determining whether the Mn-enrichment system was active in the distant past or is still active (Liu and Broecker, 2000; Perry and Adams, 1978; Perry and Hartmann, 2006; Perry and Sephton, 2006). Iron oxides in the form of magnetite, which have been oxidised by UV and cosmic radiation and, mimic magnetite found in terrestrial rock varnish, have been detected on the dry and frigid Martian surface (Mancinelli et al., 2002). As a result, there has been a surge in interest in studying these magnetic minerals, but the number of studies investigating their magnetic properties remains limited (Clayton et al., 1990).

In astrobiology, analogue regions are well-known (Hipkin et al., 2013), but new locations are being discovered and investigated to broaden the scope of astrobiology research (Preston and Dartnell, 2014). Future space research missions can use terrestrial analogues for off-Earth conditions not only as a natural laboratory for conducting testing, but also as a home for investigating future planetary coevolution studies to better understand life's interactions with its environment (Cabrol et al., 2018). In the most adverse terrestrial conditions, astrobiological investigations combined with chemical analysis can discover life signs (Cavalazzi et al., 2018). As a result, it is critical to use terrestrial-based techniques to evaluate prospective palaeobiological reserves on Mars (Cady et al., 2003). To understand the coevolution of life and its physical and chemical surroundings, one must be able to analyse evidence of life preserved in the geologic record (Cady and Noffke, 2009). As a result, the union territory of Ladakh, located in the north-western Himalaya, India represents a cold high altitude desert environment, which is an ideal location for trans-disciplinary astrobio-geochemical investigations. Because of its higher elevation and sparse vegetation, Leh-Ladakh has lower air oxygen levels, high UV radiation, and little rainfall. This location features a variety of near-pristine extreme habitats, such as glacier deposits, dry areas, dune fields, intra dune lakes, hot springs, and salt lakes, all in a natural setting, providing an intriguing parallel to the Martian climate (Pandey et al., 2020). On the other hand, rock varnish, which could have served as a possible Mars' analogue from this site, was neglected. The majority of manganese-enhanced rock varnish research has been conducted on samples from hot, arid deserts. Therefore, to bridge that gap, the current study from the Indian subcontinent to investigate the surface

characteristics and magnetic mineral characterisation of rock varnish, from the cold, dry high-altitude region of Ladakh is critical to understand Martian ecosystem.

The presence of Fe-oxides and Mn-oxides in the rock varnish is comparable to the current scenario on Mars, where manganese coated rocks and magnetic minerals have been discovered (Lanza et al., 2014a; Liu et al., 2021; Mancinelli et al., 2002). In this paper, we present the first evidence of the magnetosomes-like entities in the varnish layer, as well as an assessment of the varnish's magnetic mineral behaviour using a previously unexplored magnetic characterisation technique. As a result, the rock varnish found in Ladakh's extreme ecology may provide critical clues for comparing Mars environmental characteristics, as it contains two crucial biogeochemical elements, Fe and Mn, which may provide explanations for several unsolved Martian mysteries.

105

106

107 ## Study area

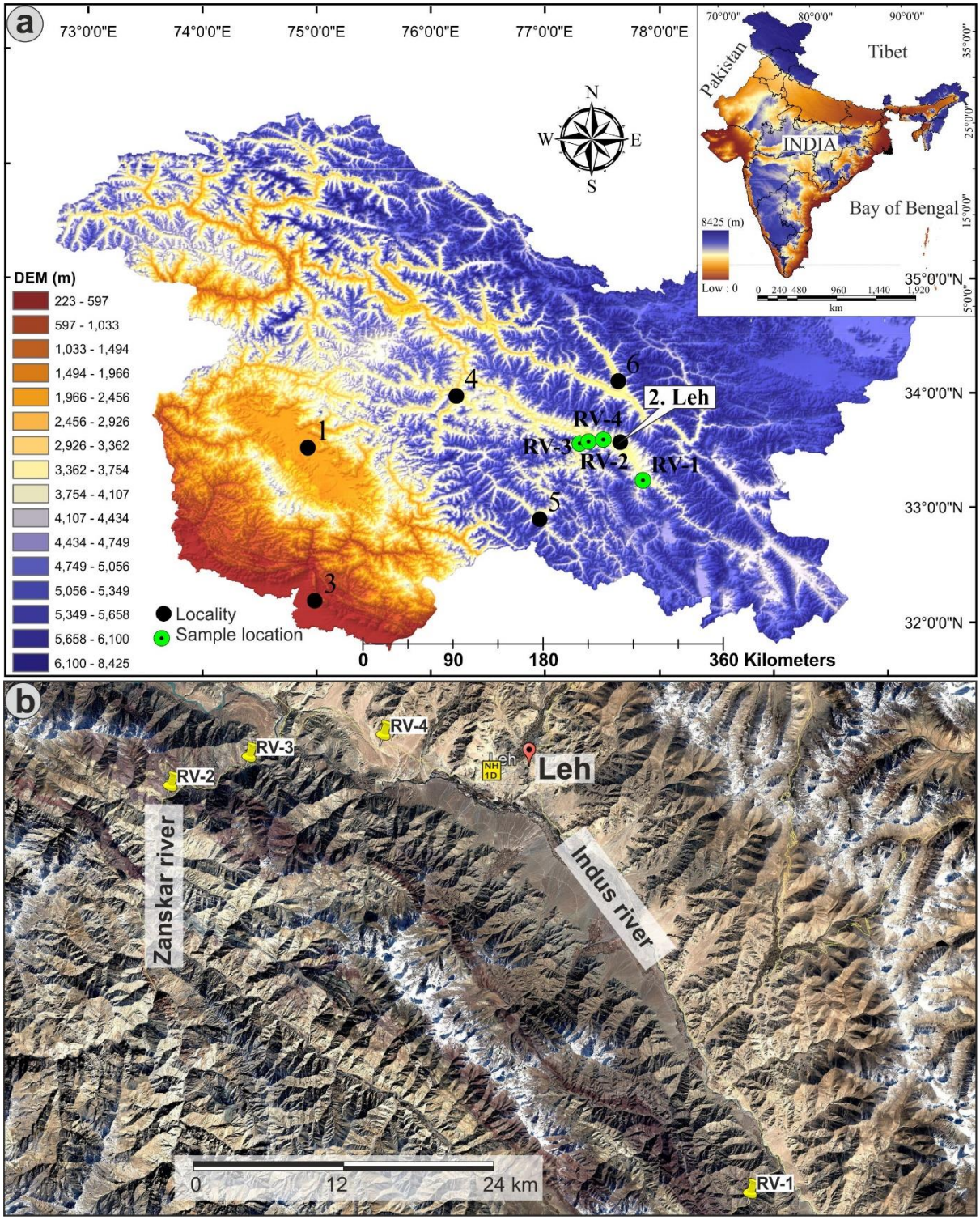

108

Fig.1. (a) Shuttle radar topography mission (SRTM) digital elevation model (DEM) showing the elevations and the location of important townships via. 1) Srinagar, 2) Leh, 3) Jammu, 4) Kargil, 5) Padum, 6) Nubra. Locations of the sample collection sites are marked by green circles. **(b)** Google Earth Pro image showing the sampling sites (yellow points RV-1, RV-2, RV-3, RV-4) as well as the Indus and Zanskar rivers with respect to Leh, Ladakh.

Fig.2 (a-d) Field photographs of the rocks sampled for rock varnish studies from NW Himalaya. The photographs from (a) to (d) represent the spots RV-1 to RV-4.

The current research was conducted in the Union territory of Ladakh, which is located in the Trans-Himalayan area (average elevation >3000 m asl) and is known as "the cold desert of India" due to its harsh semi-arid environment (Fig.1a, b) (Juyal, 2014; Norberg and Hodge, 1995; Pandey et al., 2020). Due to its location in the rain shadow zone of the Indian summer monsoon (ISM), the region receives little precipitation and has abnormally low temperatures with a wide diurnal temperature range and a short growing season (Blöthe et al., 2014; Schmidt and Nüsser, 2017). The scant vegetation in this area is due to the prevailing harsh weather conditions (Ali et al., 2018; Chaddha et al., 2021a; Sharma and Phartiyal, 2018). Ladakh has a

diverse range of accessible, diverse, clean, and harsh habitats at extremely high altitudes, including high passes that are distinct due to their altitude and, rocks exposed to 10X more UV-A doses than at sea level (Dvorkin and Steinberger, 1999). These high passes reveal a variety of comparable characteristics for early Mars due to a combination of low atmospheric pressure, strong UV, and higher UV-A doses than are today seen on Mars (Cockell, 2000). As a result, samples for this study were collected from four distinct locations in the Leh district (Ladakh), which are located between 32 and 36^{o} north latitude and 75 and 80^{o} east longitude (Fig.1a, b). The Ladakh Range (Ladakh Batholith) in the north and the Zanskar Range (Tethys Himalaya/ Indus Molasse and other rocks) in the south, form geological boundaries for the Leh district, with the contact between these two ranges generally following the Indus River. Leh has a harsh climate, with temperatures ranging from 34.8 °C in the summer to -27.9°C in the winter (Chevuturi et al., 2018).

Material method

Physicochemical characterisation

FESEM-EDS: The rock varnish samples were placed on copper stubs used for SEM examination with double-sided adhesive carbon conductive tape. To avoid cross-contamination, all mounting and other activities were carried out in a clean environment. The samples were then loaded into the JEOL 3000FC fine sputter coater, which uses nitrogen medium to deposit a thin conductive coating of Pd and Pt onto the sample surface, preventing sample charging. The coated stubs were examined with a JEOL FESEM 7610F electron microscope. Photographs of the specimens were obtained with a secondary electron detector at 15 KV acceleration volts and kept at various magnifications for analysis of the specimen's morphological traits. TEAM software was used to acquire EDS spectra from an EDAX Octane plus detector, with elemental scanning and point mapping analysis performed at 15 KV volts. Increased beam current was used to achieve a high-count rate while recording spectral analysis.

EDXRF: The elemental make-up of the varnish layer and the host rock sample was investigated using micro–X–ray fluorescence (Model: Bruker Artax 200), with a 300s life time. For molybdenum X-ray tubes, XRF scans were obtained for binary spots in the varnish layer

and the host rock, respectively, at a maximum operational voltage and current of 50 kV and 700 A.

XPS: An X-ray photoelectron spectroscopy (XPS) measurement of the varnish surface was performed on an X-ray photoelectron spectroscope (SPECS Surface Nano Analysis GmbH, Germany) using Al K radiation (1486.61 eV) X-rays, with an anode voltage of 13 kV, 100W. A survey spectrum was collected with an energy of 40 eV and high-resolution spectra were collected with an energy of 30 eV to know the valence states of the constituent elements. The extent of charging was calculated by measuring the shift of C1s peak from the reference position of 284.6 eV.

Petrographic analysis: Three representative petrographic thin sections of the Indus Molasses and one thin section of the Ladakh Batholith were examined using the Nikon Eclipse LV100POL petrological microscope.

Magnetic characterization:

The required quantity of rock varnish and the respective substrates were tightly packed in standard 8cc plastic bottles used for rock magnetic measurements. Low field magnetic susceptibility (MS), an-hysteretic remanent magnetization (ARM), saturation isothermal remanent magnetization (SIRM), and its DC demagnetization and temperature variation of magnetic susceptibility are all measured . Low frequency MS measurements were carried out with a MS2 Bartington Susceptibility meter coupled with the 2B sensor operated at a frequency of 0.47 kHz with a peak field of 200 A/m. The ARM was imparted by exposing the samples to an alternatingly decaying magnetic field of 100 mT peak field with a decay rate of 0.01 mT, in the presence of a DC bias field of 0.05 mT using a D-2000 AF demagnetizer (ASC scientific), and the ARM intensity was measured using a JR-6 dual speed Spinner magnetometer from AGICO. Saturation isothermal remanent magnetization (SIRM) was induced in a 1 Tesla steady pulsed field using an ASC Scientific Impulse Magnetizer Model IM-10-30. Backfield demagnetization was carried out at 20, 30, 100, and 300 mT pulse fields. Temperature variation of magnetic susceptibility (χ-T) was carried out using a MS2WFP Bartington sensor coupled with the MS2 meter from room temperature to 700 °C. For this, 0.20 g of samples were wrapped

with quartz paper and kept in the MS2WFP Furnace. Alternating field demagnetisation (AFD) of SIRM was performed using a D-2000 AF Demagnetiser by ASC Scientific by subjecting the samples to step-wise demagnetisation at levels of 0, 5, 10, 15, 20, 30, 40, 50, 60, 70, 80, 90, and 100 mT, respectively.

Results & Discussion

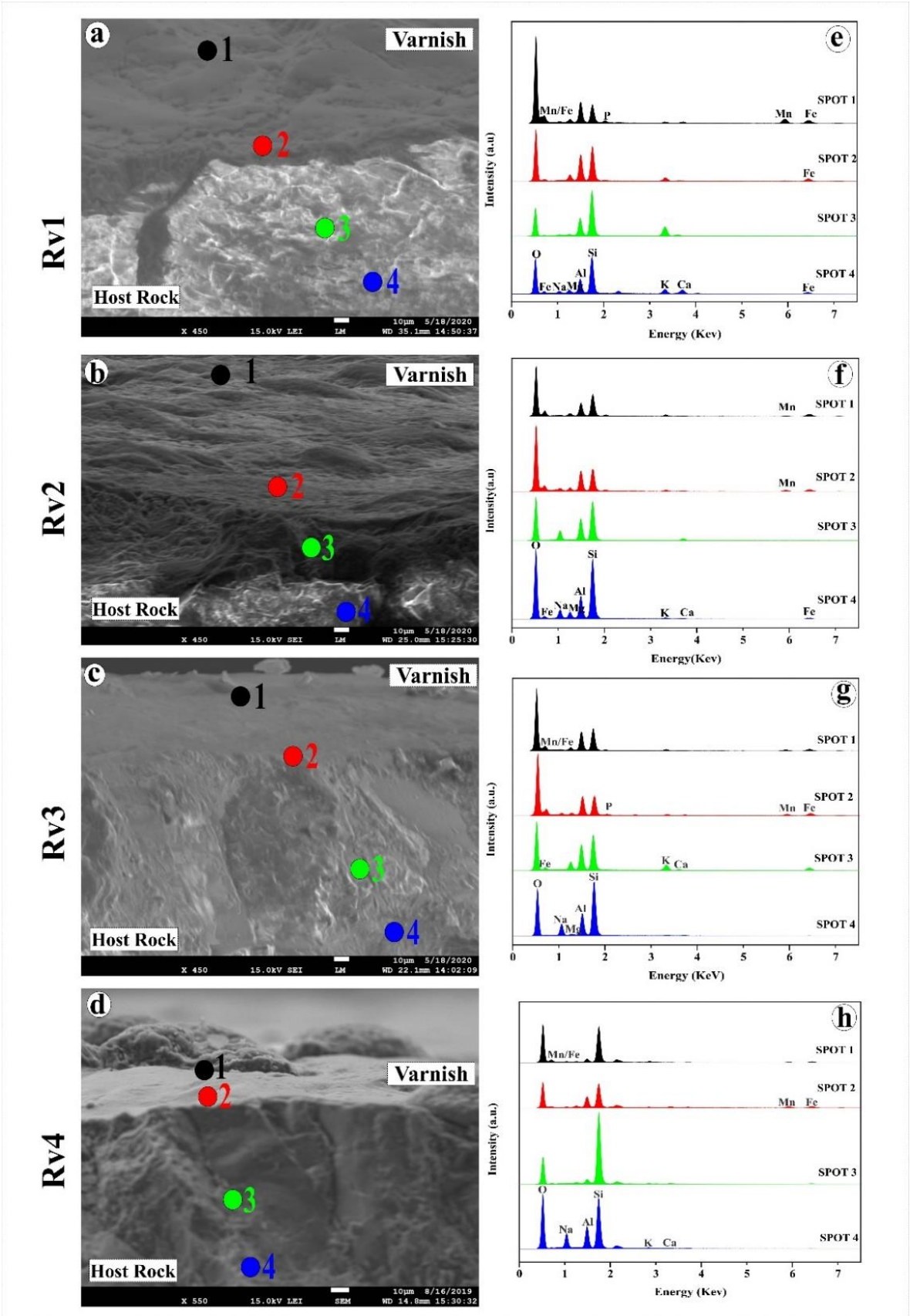

Fig.3 (a-d) FE-SEM imaging of the Rock varnish samples (RV-1 to RV-4) revealed a contrast layered morphology of the varnish layer adhered on the host rock with evident border

delimitation between the varnish layer and the host rock; Fig a,e adopted from Chaddha et al. (2021b) with permission; (e-h) Multi-spot elemental analysis of rock varnish layer and host rock revealed the elemental presence of different elements in the varnish layer and host rock with clear presence of Mn, Fe enrichment in the varnish layer.

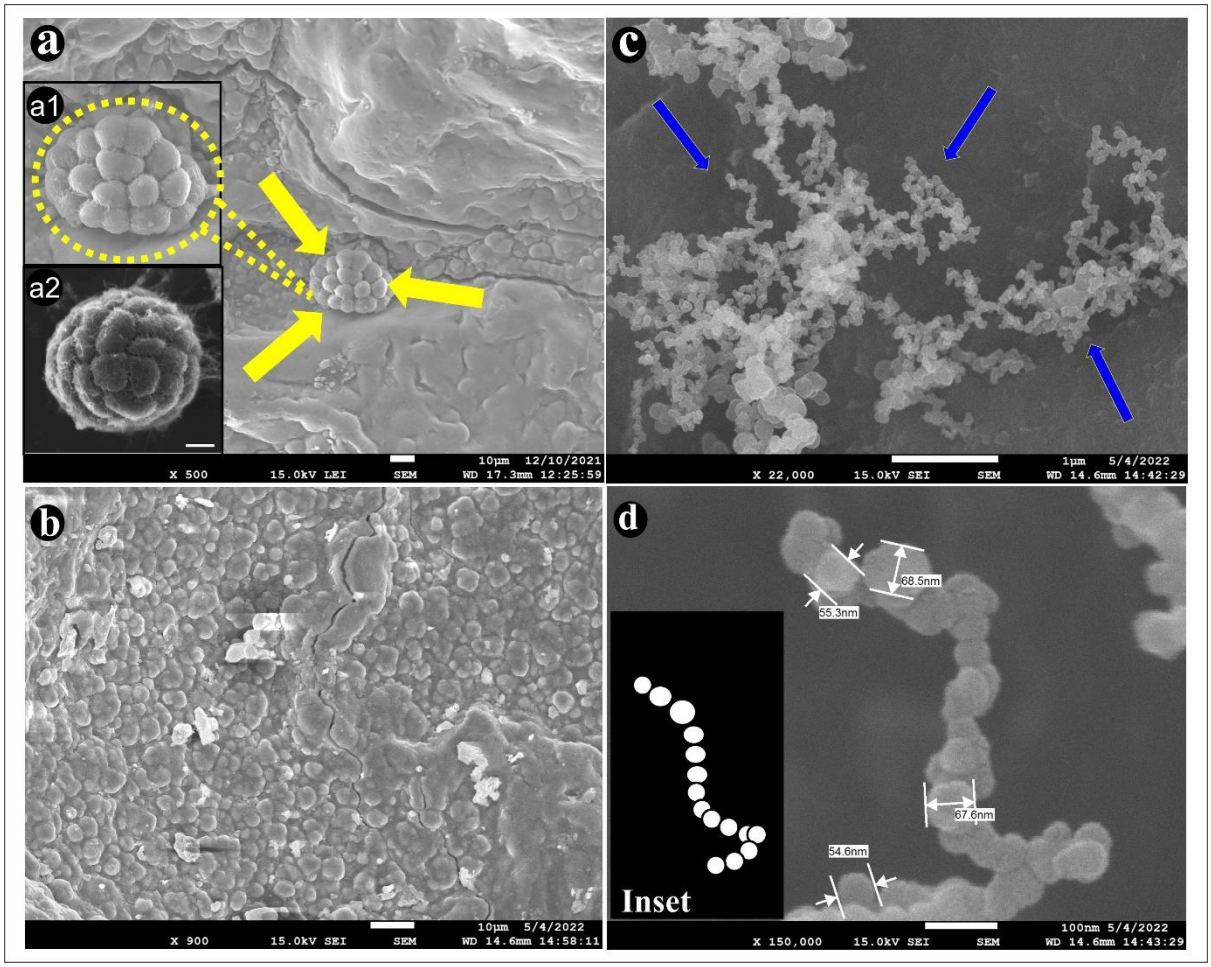

Fig.4 (a) FE-SEM image of the varnish layer showing the presence of magnetotactic multicellular aggregate (MMA) type entity embedded in the varnish layer marked by yellow arrows ; inset a1 shows magnified morphology of MMA type entity, showcasing clear morphological features; inset a2 is a SEM image of putative magnetotactic multicellular aggregate (MMA) [Used with permission of Elsevier, from Keim et al. (2004) J. Structural Biology, Vol. 145, Fig.3, p 254-262.], (b) Globules like morphological features on the varnish layer corresponding to presence of iron oxides; (c) FE-SEM image displaying clusters of chain-like established magnetosome morphology in the varnish layer; (d) High resolution FE-SEM image illustrating the chain-like morphology of putative magnetosomes present in the varnish layer, with an inset depicting a graphic description of magnetosomes' shape.

Field varnish samples (Fig.2a-d) were examined under a microscope (Fig.S1) to determine the thickness, morphology, and texture of the varnish layer. The morphological properties of the varnish layer and host rock, as well as its elemental composition, were determined by using FESEM-EDS (Field Emission Scanning Electron Microscopy-Energy Dispersive X-Ray Spectroscopy) (Figs. 3 a-h). The varnish layer and the host rock to which it was connected exhibited distinct morphologies, allowing for unambiguous demarcation of the varnish and host rock regions. A multi-spot (EDS) elemental analysis performed on the varnish and host rock layers (Fig. 3e-h) reveals the presence of various elements on the varnish layer, including Si, Al, Mg, K, Ca, O with (Mn, Fe) enrichment, and Na, Al, Si, Mg, O, and K on the host rock layer. Furthermore, the investigation revealed the existence of biotic traces in the varnish layer in the form of putative magnetotactic multicellular aggregation (MMA) type spherical organisms (Fig.4a). When the MMA found in the varnish layer (inset a1) was compared to the MMA discovered previously (inset a2) (Keim et al., 2004; Pósfai and Dunin-Borkowski, 2006; Abreu and Silva, 2008), the claims of a biotic formation route for varnish production were strengthened. These bacterial aggregates, which can function as natural machines to synthesise minerals via a biologically controlled mineralization (BCM) process, may have provided structural support and hardness to the varnish layer that we see today (Lowenstam and Weiner, 1989). In order to further validate the existence of MMA-type organisms, chain-like magnetosomes were discovered on the layer (Akbari-Karadeh et al., 2020; Kabary et al., 2017) (Fig.4 c, d; Fig.S2). Magnetosomes like entity featured on the varnish layer are in the form of chain like clusters with an average size of ~50-60 nm (Fig.4 d). The multi-spot elemental analysis of magnetosomes like entity (Fig. S3, S4) demonstrates the presence of sulphur, along with manganese and silica, indicating that the elemental chemistry analysis of these biotic entities reveals the composition of Si-Mn-S inclusions along with Fe, which goes in accordance with recent findings (Li et al., 2022). As a result, it is reasonable to assume that the generated magnetosomes like particles are made up of surface modified Fe-oxide globules, rather than the pure Fe_3O_4 (magnetite) family as previously described (Kabary et al., 2017; Liu et al., 2010). Finally, putative magnetosomes like species discovered in the varnish layer may be a new type of biotic analogue of genetically synthesised magnetic nanoparticles composed of SiO_2/Fe_3O_4 via magnetosomes (Borg et al., 2015), as the varnish layer contains all of the precursors in the form of Fe and Si required to synthesise these bio-nano magnetic particles.

These preserved biosignatures of life in the varnish layer make it an important component in the study of the Mars analogue.

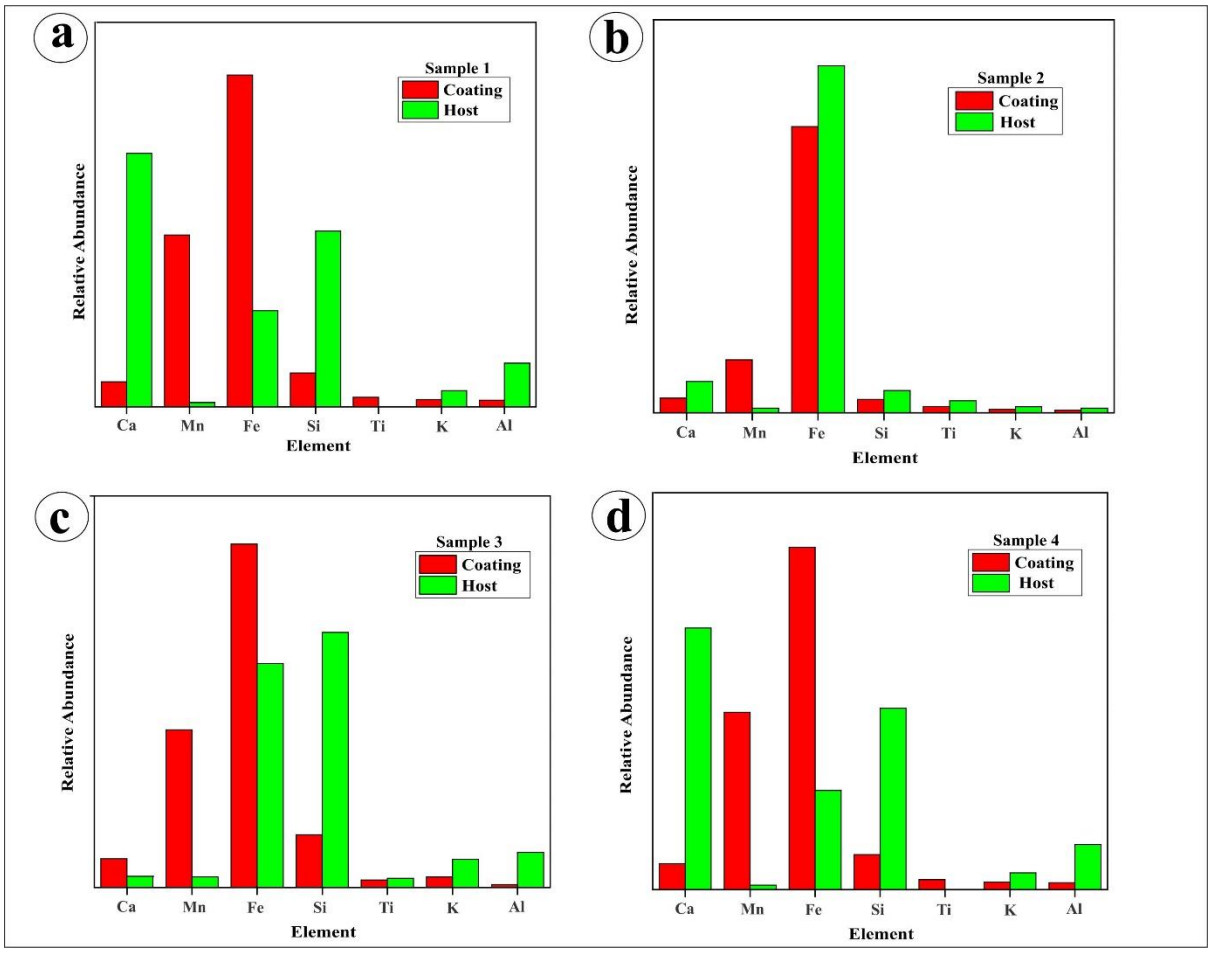

Fig.5 Comparative histograms demonstrate the relative qualitative elemental abundances between the varnish layer and the host rock samples (RV-1 to 4) using energy dispersive X-ray fluorescence analysis.

To understand the difference in relative element abundance between the varnish layer and its related host rock, micro-X-ray fluorescence spectroscopy with simultaneous multi-element analysis was applied to the varnish and host rock surface of the samples (Fig.5a, b, c, d). The presence of Si in the varnish layer is lower than in the host rock, whereas Mn and Fe are higher. Fe and Mn are more common in the varnish layer than in the rock it covers, which suggests that they are the most important parts of the varnish layer.

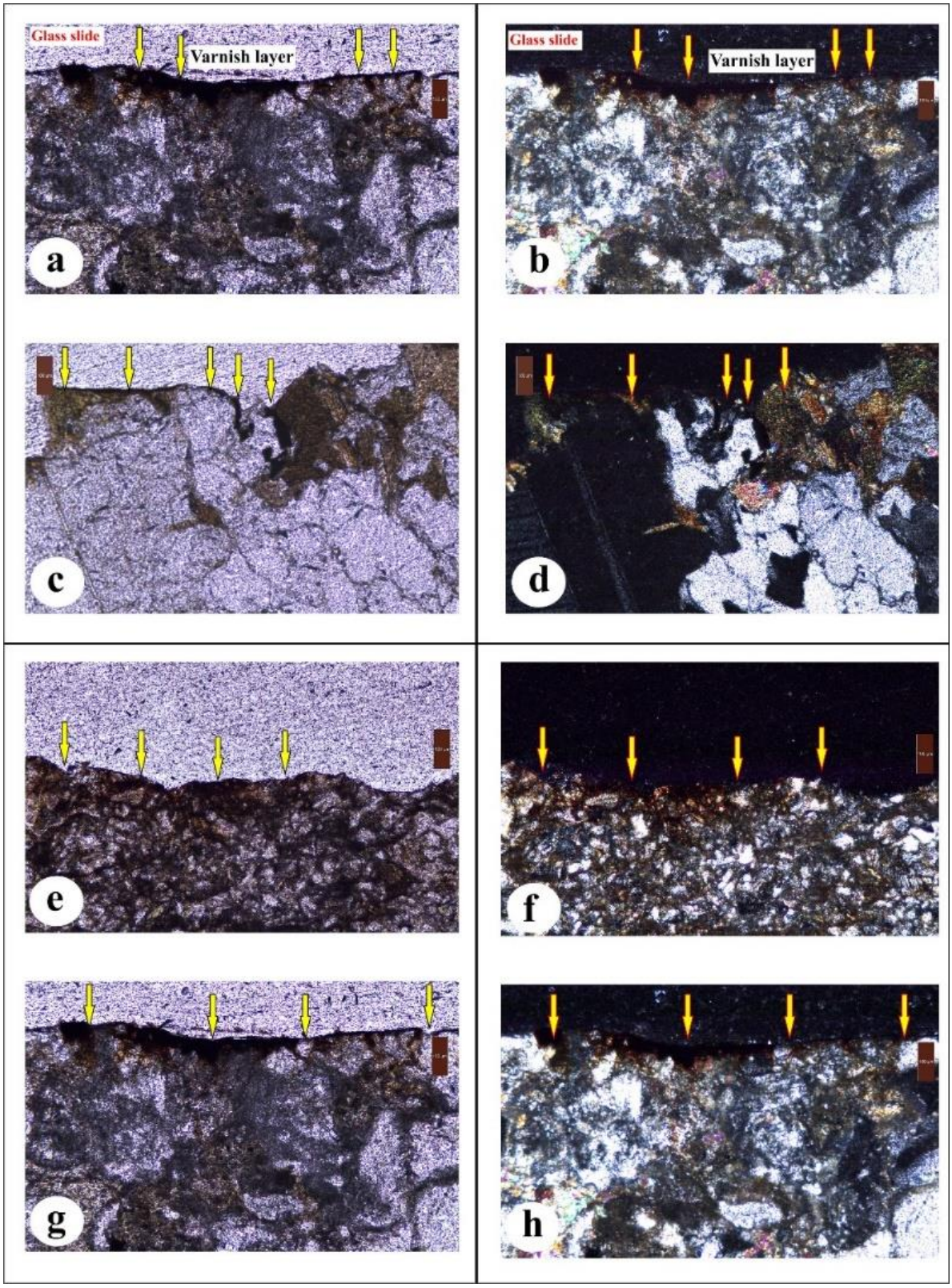

Fig.6 (a, c, e, g) Thin section slides of a cross-section of varnish samples (RV1, RV2, RV3, RV4) in plane-polarized light at 10x; (b, d, f, h) Thin section slides of a cross-section of varnish samples (RV1, RV2, RV3, RV4) in crossed polarized light at 10x. The thin micro varnish coating is indicated by yellow arrows.

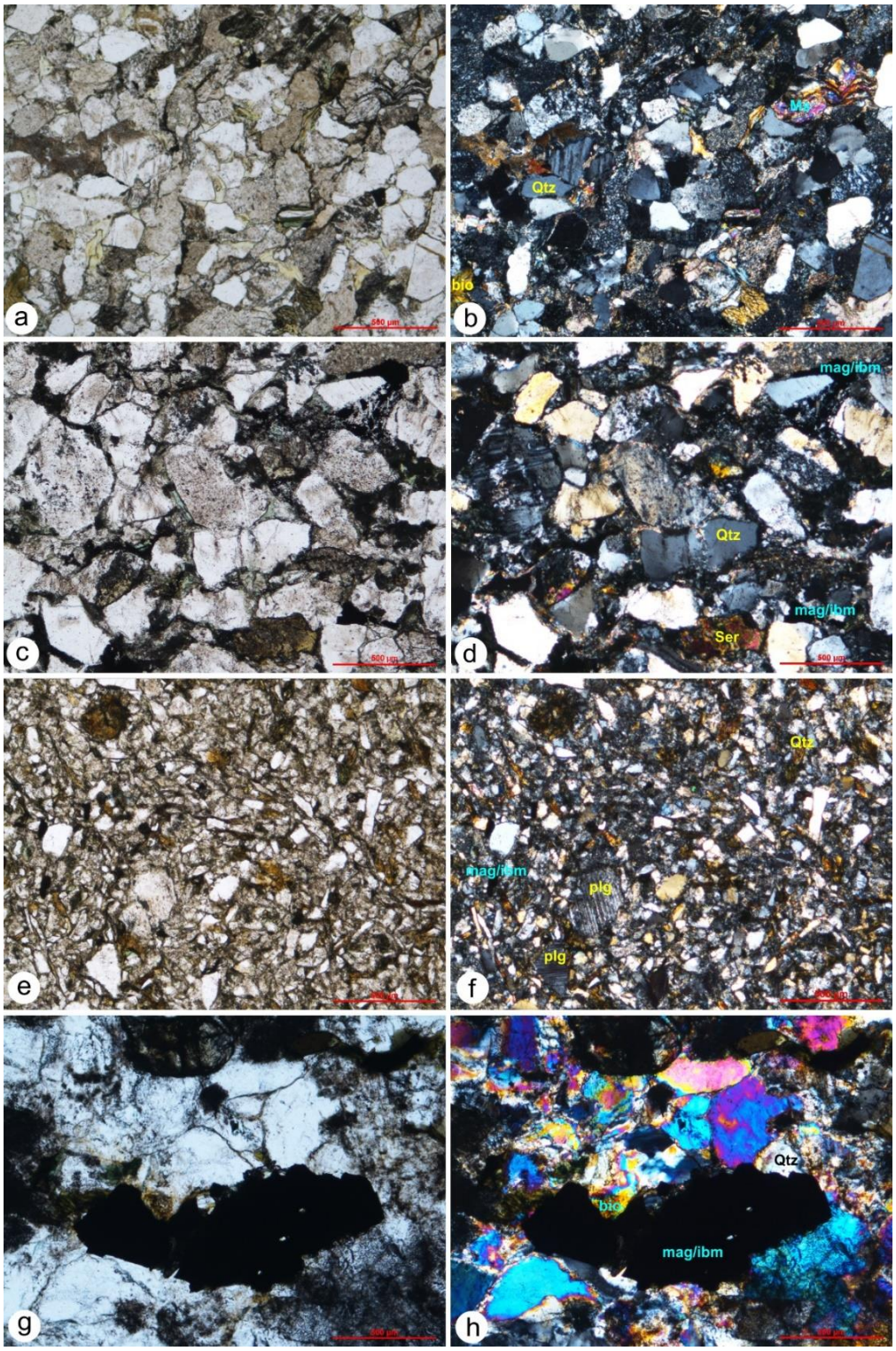

Fig 7. Petrographic thin sections demonstrate host rock characteristics. a-f: Indus molasses (RV1, RV2, RV3); g-h: Ladakh Batholith (RV4). a, c, e, and g: in 4x plane polarised light. b, d, f, and h: in 4x cross polarised light. Abbreviations: Qtz – quartz; plg – plagioclase; Ms – muscovite; mgm/ibm – magnetite/iron bearing mineral; bio – biotite; Ser – Sericite.

Petrographic examination of cross-thin sections of varnished rock samples (Fig. 6) was used to identify the micro layer of varnish adhering to the associated host rock, which was visible in plane polarised light (Fig.6 a, c, e, g). However, the black-brown texture of the layer in both plane polarised light and under cross nicol, showing the presence of opaque minerals such as iron containing minerals in the varnish layer, did not provide a complete array of identification. A detailed petrological analysis was done to understand the mineralogical composition of the various substrates on which varnish is deposited (host rock) (Fig.7). Figures a-f depict the Indus Molasse (sedimentary), while g-h depict the Ladakh Batholith (igneous), both of which are completely different types of rocks in terms of origin and mineral content. Magnetite/ibm, an opaque mineral, has been observed by petrographic examination in both types of host rock. In the Indus Molasses (Fig. 7 a-f), magnetite/ibm comprises up 1- 2% of the entire grain population, but more than 15% in the Ladakh Batholith (Fig.7 g-h). A detailed petrographic investigation of the host rock's mineralogical characterization can be found in the supplementary information under the heading (HS.1).

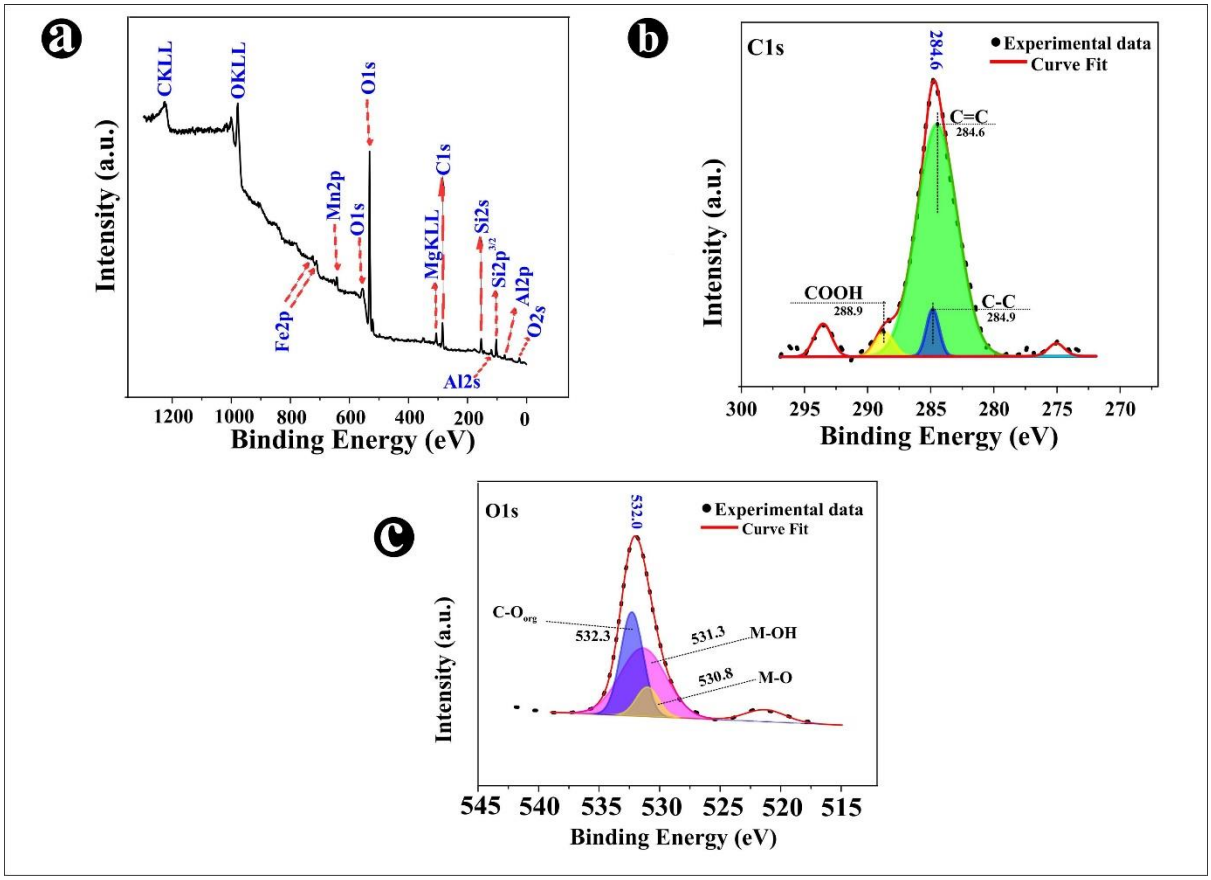

Fig.8 (a) A wide range XPS survey spectrum of the rock varnish surface reveals elements on the varnish layer; (b) XPS spectra of core level C1s from the varnish surface;(c) XPS spectra of core level O1s from the varnish surface.

By utilising the XPS technique to examine the surface of rock varnish, the elemental makeup and oxidation states of the elements present at the varnish's surface are revealed. The surface electronic states and chemical composition are visible in the XPS survey spectra (Fig.8a), with the presence of Fe, Mn, O, C, Al, Si, and Mg owing to its natural origin. The peak at 284.6 of C1s was carefully used as a referencing method for charge correction as recommended by ISO and ASTM charge referencing guides (ASTM E1523-15, 2015; Baer, 2005; Greczynski and Hultman, 2020). Furthermore, deconvolution of C1s XPS spectra (Fig.8b) yielded three distinct Lorentzian–Gaussian curves centred at binding energies of 284.6 eV, 284.9 eV, and 288.9 eV of C=C, C-C, and -COOH groups respectively (Rabchinskii et al., 2018). Because carboxylic acid molecules are prevalent in microbial metabolic pathways, the presence of carboxylic group functionality in the varnish layer suggests microbial presence on the layer (Booth et al., 2002; Magnuson and Lasure, 2004; Mira and Teixeira, 2013). Furthermore, a peak at ~293.0 eV in the C1s spectra indicates the existence of K, in addition to the other

elements discovered in the XPS survey scan (Fig.8a). The deconvolution peaks of the O1s spectrum (Fig.8c) may be separated into three components: lattice oxide (M-O, 530.8 eV), surface hydroxyl (M-OH, 531.3 eV) and organic moiety (C-O, 532.3 eV), respectively (Biesinger et al., 2010; Luo et al., 2022). The presence of organic functionality (Rouxhet and Genet, 2011), as well as Mn and Fe cemented with clay minerals (Chaddha et al., 2021b), supports varnish-rich rocks as a good terrestrial comparison for understanding the Martian environment and its hints for biotic life signs.

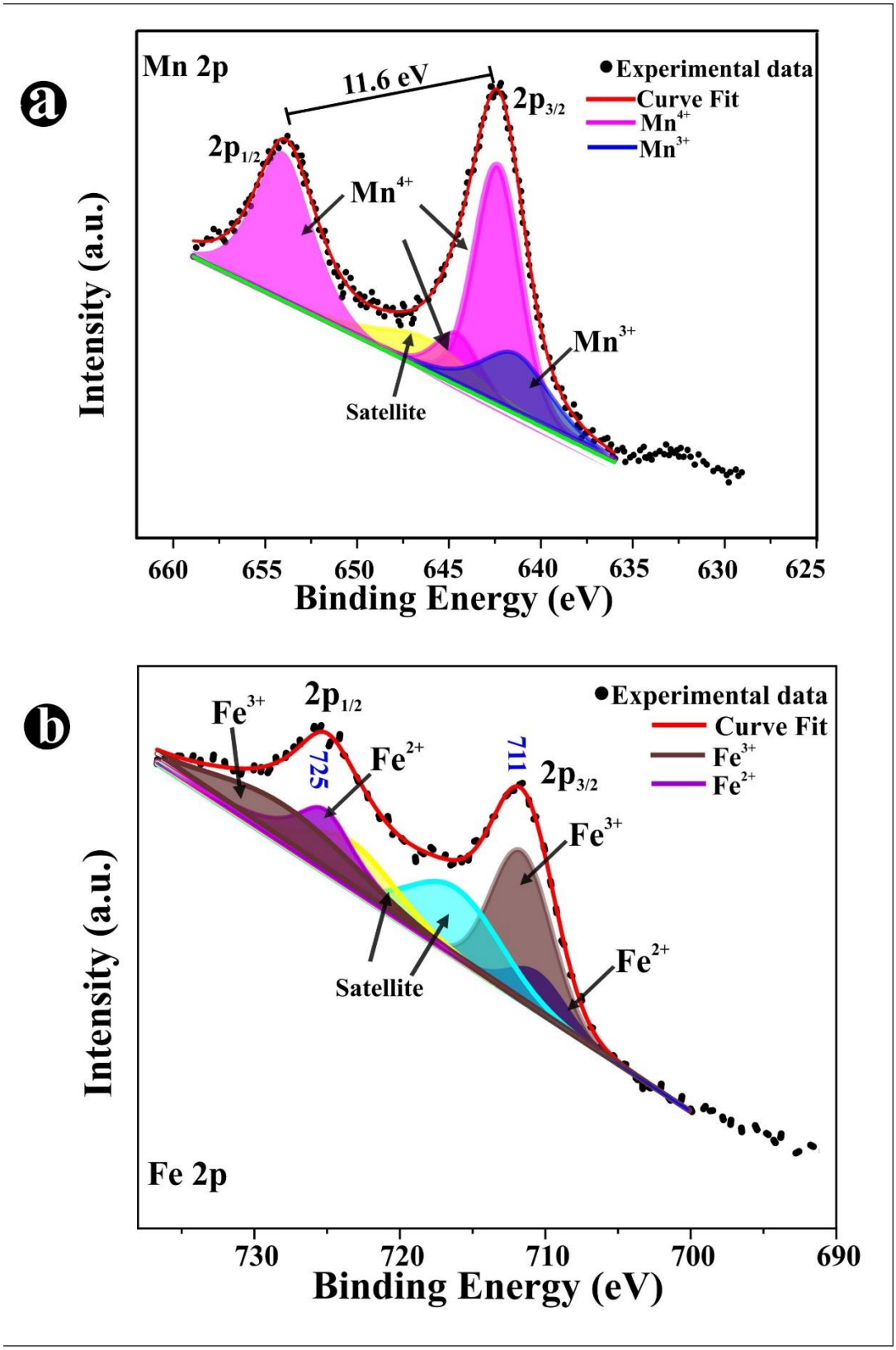

Fig. 9 (a) High-resolution Mn 2p core-level spectra of the varnish layer with Mn 2p peak splitting into the Mn $2p_{3/2}$ peak and Mn $2p_{1/2}$ peak; (b) High-resolution Fe 2p core-level spectra of the varnish layer, with Fe 2p peak splitting into the Fe $2p_{3/2}$ peak and Fe $2p_{1/2}$ peak.

Previous studies have shown the presence of Mn and Fe on the Martian rocks (Lanza et al., 2014b; Rochette et al., 2006), so a high resolution XPS spectrum study of Mn and Fe for the varnish layer was reported (Fig.9a, b). Mn2p spectrum reveals two spin orbit doublets of Mn $2p_{3/2}$ and Mn $2p_{1/2}$ at 642.4 eV and 654.0 eV respectively with a peak separation of 11.6 eV (Fig. 9a), which are in good agreement with those reported for Birnessite type -MnO_2 (Biesinger et al., 2010; Cremonezzi et al., 2020; Ilton et al., 2016; Nesbitt and Banerjee, 1998), indicating existence of Mn^{4+} oxidation state. The deconvolution of spin–orbit peaks indicate the co-existence of Mn^{4+} and Mn^{3+} valence states at 642.4 and 641.4 eV, respectively. However, the peak corresponding to the Mn^{4+} state, on the other hand, has a higher peak intensity and a larger area under the curve than the peak corresponding to the Mn^{3+} state, indicating that the sample contains a main phase as MnO_2 and a partially surface oxidised Mn phase (John et al., 2016; Singh et al., 2019). The Mn valence composition was determined by fixing the FWHM of multiplets (Sun et al., 2016), with peak fitting parameters of Mn^{4+} (FWHM=2.97 eV, χ^2=0.64) and Mn^{3+} (FWHM=4.45 eV, χ^2=0.64) respectively, where Mn^{4+} was (82%) and Mn^{3+}(18%). These results further substantiate the presence of birnessite phase in the varnish layer in accordance with the recent report of manganese oxide minerals at shallow terrestrial depths (Yun et al., 2022), Birnessite phase in the varnish layer is also consistent with (Chaddha et al., 2022). Initially, biogenic birnessite is hypothesised to originate as δ-MnO_2, a type of birnessite. According to laboratory experiments, this variety of birnessite is always the first phase to form under most tested chemical settings (Hansel et al., 2012; Santelli et al., 2011; Villalobos et al., 2006, 2003). Due to the existence of interstitial vacancies in the lattice, birnessite can also play a role in transition metal sorbers (Kwon et al., 2010; Toner et al., 2006). Therefore , layered Mn oxide minerals of the birnessite family are being studied in depth for their natural occurrence and chemical reactivity in a range of terrestrial environments (Ling et al., 2020). As a result, this mineral could be useful in analysing changes in Martian analogue settings.

Analysis of a high resolution Fe2p XPS spectra of Fe present in the varnish layer (Fig.9b) suggests the presence of Fe (II)/Fe (III) oxides, with peak locations of ~711 eV and ~725 eV of Fe 2p3/2 and Fe 2p1/2, respectively. The existence of these spectral peaks indicates that both haematite and magnetite minerals are present in the varnish layer (Yamashita and Hayes, 2008). The existence of satellite peaks in the varnish layer lends credence to the presence of haematite phase (Mills and Sullivan, 1983; Muhler et al., 1992). Further deconvolution of Fe $2p_{3/2}$ and Fe $2p_{1/2}$ produces Fe^{2+} and Fe^{3+} states with atomic ratios of Fe^{3+}(0.68) and Fe^{2+} (0.31)

respectively, which is consistent with earlier magnetite results (Yamashita and Hayes, 2008). Peak fit parameters of Fe^{3+} (FWHM=4.85 eV, χ^2=0.76) and Fe^{2+} (FWHM=4.58 eV, χ^2=0.76) were also observed. As a result , surface analysis of the varnish layer confirms the role of Fe-oxides in the form of magnetite and hematite in giving the rock varnish a reddish brown texture, similar to that found in various locations on Mars (Jiang et al., 2022). Therefore, the presence of Mn and Fe in the rock varnishes makes them a promising model for studying the Martian climate and chemical environment, which can be clearly seen in images (Fig. 10). Furthermore, Mn and Fe are two biologically abundant elements found in the majority of key biological cycles on Earth, which may provide insight into the genesis of life on Mars (Clark et al., 2021; Krinsley et al., 2009; Tan and Sephton, 2020).

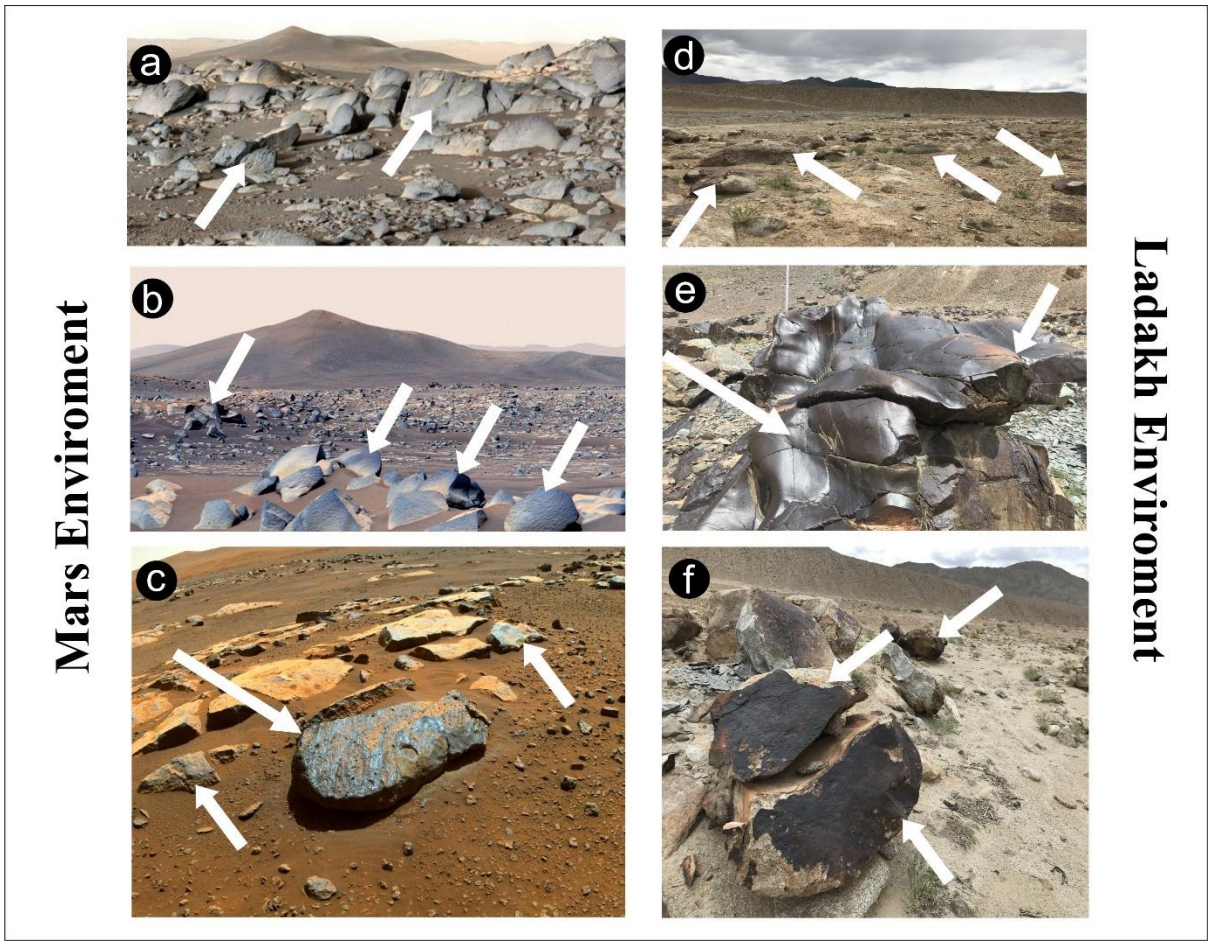

Fig.10 A view from the NASA's Mars rover showing a boulder field in front of a location named as “Santa Cruz”; (b) NASA's Perseverance Mars rover obtained this image of "Santa Cruz" hill in Jezero Crater by stitching together 24 separate photographs from the rover's Mastcam-Z camera system, the rover crew called the boulders in the foreground "Ch'al" rocks;

(c) The Perseverance rover obtained this image of "Rochette" shortly after abrading "Bellegarde," a circular region of Martian rock 2 inches in diameter and 0.39 inch in depth. Image Credit (a-c): NASA/JPL-Caltech; (d) synoptic view of barren landscape with varnish coated boulders; (e) Thick glazed shining brown varnish coating on Ladakh rocks; (f) Rich dark reddish-brown coating on Ladakh batholith boulders.

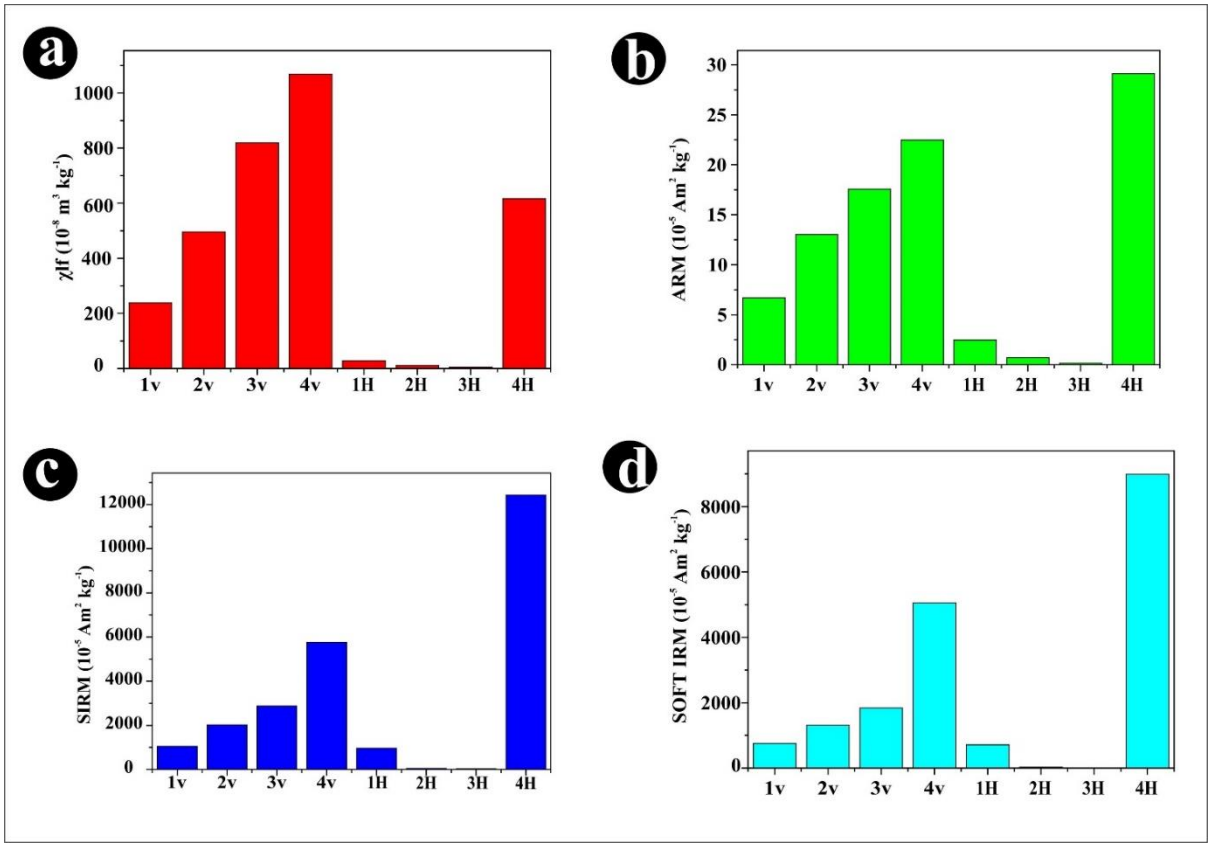

Fig.11 Magnetic concentration dependent parameters show a clear contrast in magnetic concentration between the varnish and the associated host rock.

The presence of Fe-oxides in the varnish layer was investigated further by magnetic characterization of the varnish sample to determine the varnish's magnetic behaviour in relation to its host rock. The rock varnishes are more magnetic than their substrates (host rock), according to low frequency magnetic susceptibility (χ_{lf}) data, which is a measure of the concentration of magnetic minerals in a sample. The varnish samples 1V, 2V, and 3V have substantially more χ_{lf} than their substrates 1H, 2H, and 3H; however, 4V has similar magnetic susceptibility to its substrate 4H. Furthermore, the two magnetic concentration-dependent metrics, ARM and SIRM, show that the varnish layers have identical magnetic concentrations (Fig.11b-d). This difference in sample 4 can be attributed to its igneous origin, as it was collected from the northern flank of the Indus River/valley, which is composed of igneous boulders (Ladakh batholith). This would imply that the substrate contains magnetite grains, as evidenced by petrographic studies (Fig.7g, h). The susceptibility levels of varnish samples' are much higher than any literature documented in the Leh-Ladakh region (Phartiyal et al., 2021,

2020; Sangode et al., 2013). It could be linked to the concentration enrichment of the magnetic minerals on the varnish layer, as well as a possible biological origin for the varnish formation process (Chen et al., 2021). In a previous study, varnished and unvarnished wafers from three geologically distinct rock samples showed that rocks with high intrinsic magnetization have no discernible behaviour between the varnish and host, whereas rocks with lower intrinsic magnetization have distinct and reproducible differences between the varnish and unvarnished wafers (Clayton et al., 1990), which is consistent with the current findings. The S-ratio parameter S300 (Calculated as |IRM-300 mT|/SIRM), which analyses the relative proportion of hematite to magnetite in a sample is close to 1, suggesting that varnish layers are primarily composed of magnetite minerals. The S-ratio of 0.81 indicates that a small proportion of antiferromagnetic minerals are present in sample 2V of rock varnish (Table S1). A ratio of 1 indicates that the ferrimagnetic mineral magnetite is the primary remanence carrier, and as the proportion of hematite in a mixture increases , the S-ratio decreases (Basavaiah and Khadkikar, 2004; Bloemendal et al., 1992; Liu et al., 2012). Temperature variation magnetic susceptibility scans (χ-T) in samples RV1, RV2, and RV3, on varnish and host rock are less resolvable. However, in sample RV4, both varnish and host rock have the same mineralogy of a strong magnetite phase (a sharp decrease in susceptibility values between 550 and 600 °C) and a minor hematite phase (680 °C) (Fig.S5). The remnant coercivity spectrum and magnetic mineralogy were also determined using IRM acquisition and demagnetisation studies. Because the IRM acquisition curves were saturated around 200 mT field values, these curves (Fig.12a-d) imply a substantially ferrimagnetic phase of the varnish and the host rock. Remanence coercivity (Hcr) values of 18-22 mT for varnishes and 40-60 mT for host rocks, on the other hand suggested a change in magnetic grain size. This leads to the premise that the varnish layer may be composed of coarser multidomain (MD) magnetite(~110μ) and the host rock of a pseudo single domain (PSD) magnetite(~0.2-110 μ) in nature(Walden, 1999; Yang et al., 2010). This is substantiated by the AF Demagnetisation examinations that have been conducted. Normalized data from SIRM Stepwise AF Demagnetization curves (Fig. 13 a-d) demonstrate that the varnish sample is relatively easy to demagnetize (Dunlop et al., 2004). These results further validate and refine the categorization of magnetite grains found in the varnish layer with birnessite and haematite, as described in a previous study comparing magnetite in the rock varnish and its applicability to Mars (Mancinelli et al., 2002). Varnish and its substrate (host rock) have different magnetic domain sizes, which may provide insight into the varnish formation process, as multidomain coarser grain sizes are indicative of secondary depositional processes with a slow rate of accumulation and growth, as opposed to single domain grain

sizes, which have signatures of a rapid rate of nucleation and crystallisation as seen in host rocks (Stacey, 1961). As a result, the magnetic mineral concentration and grain size of varnish and host rock differ significantly, with a dominating ferrimagnetic mineral assemblage.

Overall, the presence of highly oxidised Mn and Fe in the varnish layer from extreme terrestrial environments, as well as microbial entities, makes rock varnish an important subject of study for linking past climatic conditions on Mars. The presence of iron and manganese oxide rich patinas on Martian rocks supports the claims of an oxygen-rich environment on Mars in the past, which lends credence to the story about Mars previous habitability. Ladakh could be a feasible location for both early and modern Mars scenarios, as it possesses water features such as lakes and rivers similar to those found on early Mars (4 billion years ago), as well as cold, dry surface characteristics with a high UV flux today. As a result, rock varnish can aid in the understanding of life's co-evolution and the prediction of Mars and Earth's past, present, and future climates. The preceding discussion introduced the key question whether, if Mars and the Earth are closely related, Earth would experience a similar fate to that of present-day Mars, characterised by low O_2 and high CO_2 concentrations.

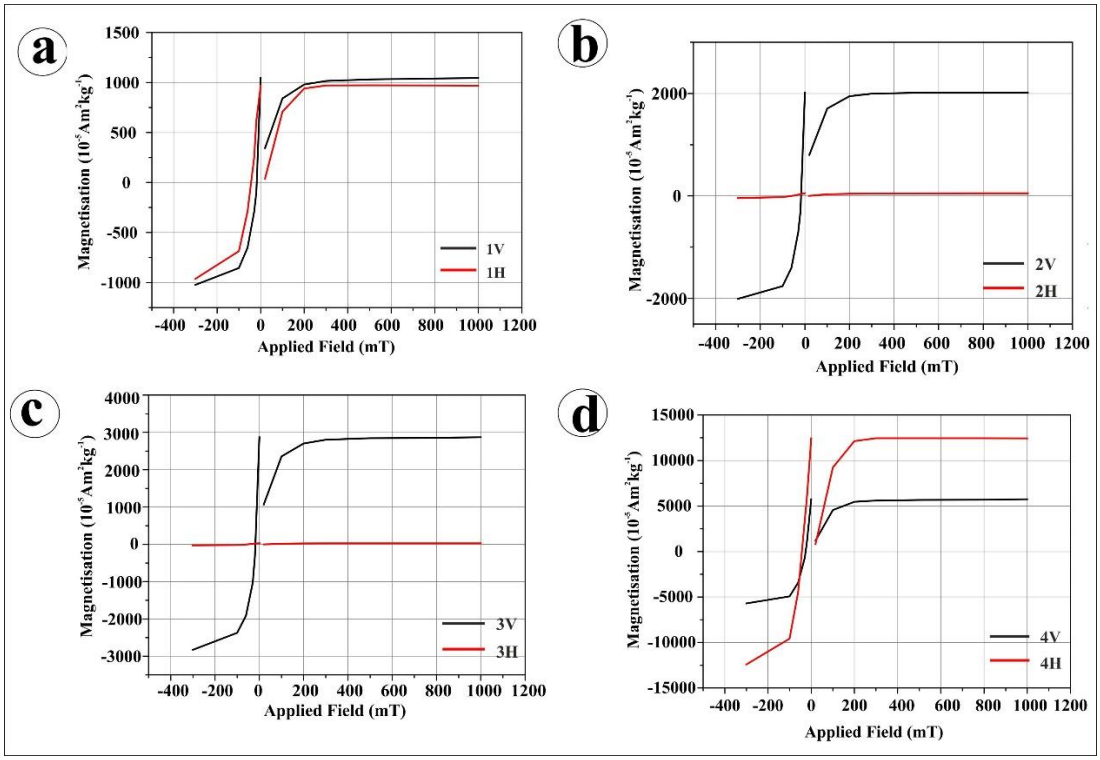

Fig.12 Stepwise IRM acquisition and demagnetisation curves revealing the samples' principal ferrimagnetic phase .

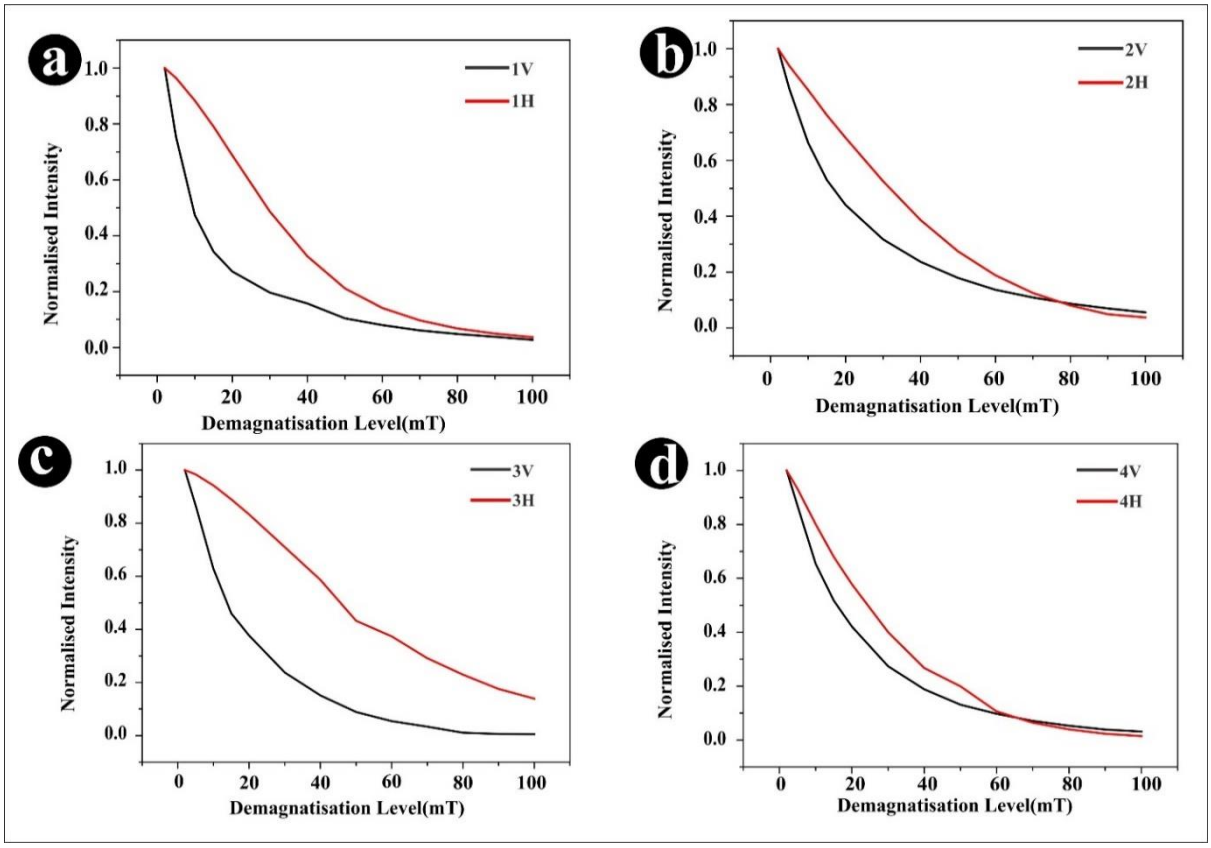

Fig.13 AF Demagnetisation of SIRM revealing a relatively harder remanent component of the host rocks compare to respective varnishes.

Conclusion

With intense solar UV radiation, vast temperature changes, and a cold arid environment, Ladakh hosts an ideal planet analogous setting (PAS) for understanding the biogeochemical fingerprints of modern-day Mars. The dark reddish-brown coatings found on many rocks in Ladakh were identical to those found on Mars during the recent mission of the Perseverance rover. The existence of Fe and Mn in the varnish layer, which accommodates a chain of biologically driven new types of magnetosomes like species formed of Si-Mn-S inclusions together with Fe, is suggested by the surface and magnetic characteristics of rock varnish. The presence of magnetic minerals in the varnish layer with a larger fraction of oxidised Fe^{3+} and Mn^{4+} cations could provide an answer to the long-standing debate of whether Mars had oxic conditions in the past or not. This evidence is enhanced when combined with the findings of the Curiosity rover's ChemCam instrument, which discovered manganese oxide veins and manganese-rich coatings on Martian rocks while operating. As a result, the role of Mn and Fe

oxides in the varnish layer as well as the microbiota that flourishes over the varnish layer must therefore be extensively examined. As such, we suggest that the typical rock varnishes from extreme environmental places like Ladakh, India may provide a significant piece of the puzzle of life beyond the Earth.

Acknowledgment

The work presented in the manuscript is part of the doctoral thesis work of A.S.C. The authors thank Director, BSIP, for providing encouragement and all necessary support for the work. We particularly thank the BSIP-SAIF Facility for providing access to analytical facilities needed in the study. The authors acknowledge Dr. Uday Deshpande of DAE-UGC-Indore for conducting XPS studies. We express special thanks to Dr. Preeti Verma for carrying out the ED-XRF analysis.

Author(s') disclosure (Conflict of Interest) statement(s)

The authors declare no competing interests.

Funding statement

This research received funding from BSIP-Lucknow, India.

References

Abreu F and Silva K. Greigite Magnetosome Membrane Ultrastructure in 'Candidatus Magnetoglobus Multicellularis.' International Microbiology 2008;(11):75–80; doi: 10.2436/20.1501.01.46.

Akbari-Karadeh S, Aghamiri SMR, Tajer-Mohammad-Ghazvini P, et al. Radiolabeling of Biogenic Magnetic Nanoparticles with Rhenium-188 as a Novel Agent for Targeted Radiotherapy. Appl Biochem Biotechnol 2020;190(2):540–550; doi: 10.1007/s12010-019-03079-x.

Ali SN, Thakur B, Morthekai P, et al. DIATOM DIVERSITY UNDER EXTREME CLIMATE: A STUDY FROM ZANSKAR VALLEY, NW HIMALAYA, INDIA. 2018;8.

ASTM E1523-15. Standard Guide to Charge Control and Charge Referencing Techniques in X-Ray Photoelectron Spectroscopy. 2015.

Baer DR. Summary of ISO/TC 201 Standard: XVIII, ISO 19318: 2004—Surface Chemical Analysis—X-ray Photoelectron Spectroscopy—Reporting of Methods Used for Charge Control and Charge Correction. Surface and Interface Analysis: An International Journal devoted to the development and application of techniques for the analysis of surfaces, interfaces and thin films 2005;37(5):524–526.

523 Basavaiah N and Khadkikar A. Environmental Magnetism and It's Application towards
524 Palaeomonsoon Reconstruction. J Ind Geophys Union 2004;8.

525 Biesinger MC, Lau LWM, Gerson AR, et al. Resolving Surface Chemical States in XPS Analysis of First
526 Row Transition Metals, Oxides and Hydroxides: Sc, Ti, V, Cu and Zn. Applied Surface Science
527 2010;257(3):887–898; doi: 10.1016/j.apsusc.2010.07.086.

528 Bloemendal J, King JW, Hall FR, et al. Rock Magnetism of Late Neogene and Pleistocene Deep-Sea
529 Sediments: Relationship to Sediment Source, Diagenetic Processes, and Sediment Lithology. Journal
530 of Geophysical Research: Solid Earth 1992;97(B4):4361–4375; doi: 10.1029/91JB03068.

531 Blöthe JH, Munack H, Korup O, et al. Late Quaternary Valley Infill and Dissection in the Indus River,
532 Western Tibetan Plateau Margin. Quaternary Science Reviews 2014;94:102–119; doi:
533 10.1016/j.quascirev.2014.04.011.

534 Booth IR, Cash P and O'Byrne C. Sensing and Adapting to Acid Stress. Antonie Van Leeuwenhoek
535 2002;81(1):33–42; doi: 10.1023/A:1020565206835.

536 Borg S, Rothenstein D, Bill J, et al. Generation of Multishell Magnetic Hybrid Nanoparticles by
537 Encapsulation of Genetically Engineered and Fluorescent Bacterial Magnetosomes with ZnO and SiO_2
538 . Small 2015;11(33):4209–4217; doi: 10.1002/smll.201500028.

539 Cabrol NA, Grin EA, Bishop JL, et al. Concluding Remarks: Bridging Strategic Knowledge Gaps in the
540 Search for Biosignatures on Mars—A Blueprint ☆. In: From Habitability to Life on Mars Elsevier;
541 2018; pp. 349–360; doi: 10.1016/B978-0-12-809935-3.00014-1.

542 Cady S and Noffke N. Geobiology: Evidence for Early Life on Earth and the Search for Life on Other
543 Planets. GSAT 2009;4–10; doi: 10.1130/GSATG62A.1.

544 Cady SL, Farmer JD, Grotzinger JP, et al. Morphological Biosignatures and the Search for Life on
545 Mars. Astrobiology 2003;3(2):351–368; doi: 10.1089/153110703769016442.

546 Cavalazzi B, Glamoclija M, Brack A, et al. Astrobiology, the Emergence of Life, and Planetary
547 Exploration. In: Planetary Geology. (Rossi AP and van Gasselt S. eds) Springer International
548 Publishing: Cham; 2018; pp. 347–367; doi: 10.1007/978-3-319-65179-8_14.

549 Chaddha AS, Mathews RP, Kumar K, et al. Caves as Interim-Refugia: Chemical Signatures of Human
550 Habitation under Extreme Environments of Ladakh, NW India. Journal of Archaeological Science:
551 Reports 2021a;36:102799; doi: 10.1016/j.jasrep.2021.102799.

552 Chaddha AS, Sharma A and Singh NK. Clay Minerals Identification in Rock Varnish by XRD: A One-
553 Step Reduction Approach. MethodsX 2021b;8:101511; doi: 10.1016/j.mex.2021.101511.

554 Chaddha AS, Singh NK, Malviya M, et al. Birnessite-Clay Mineral Couple in the Rock Varnish: A
555 Nature's Electrocatalyst. Sustainable Energy Fuels 2022; doi: 10.1039/D2SE00185C.

556 Chen L, Wang M, Li Y, et al. Effects of Magnetic Minerals Exposure and Microbial Responses in
557 Surface Sediment across the Bohai Sea. Microorganisms 2021;10(1):6; doi:
558 10.3390/microorganisms10010006.

559 Chevuturi A, Dimri AP and Thayyen RJ. Climate Change over Leh (Ladakh), India. Theor Appl Climatol
560 2018;131(1–2):531–545; doi: 10.1007/s00704-016-1989-1.

561 Clark BC, Kolb VM, Steele A, et al. Origin of Life on Mars: Suitability and Opportunities. Life
562 2021;11(6):539; doi: 10.3390/life11060539.

563 Clayton JA, Verosub KL and Harrington CD. Magnetic Techniques Applied to the Study of Rock
564 Varnish. Geophysical Research Letters 1990;17(6):787–790; doi: 10.1029/GL017i006p00787.

565 Cockell C. The Ultraviolet Environment of Mars: Biological Implications Past, Present, and Future.
566 Icarus 2000;146(2):343–359; doi: 10.1006/icar.2000.6393.

567 Cremonezzi JM de O, Tiba DY and Domingues SH. Fast Synthesis of δ-MnO2 for a High-Performance
568 Supercapacitor Electrode. SN Appl Sci 2020;2(10):1689; doi: 10.1007/s42452-020-03488-2.

569 Dorn RI and Oberlander TM. Microbial Origin of Desert Varnish. Science 1981; doi:
570 10.1126/science.213.4513.1245.

571 Dunlop DJ, Xu S and Heider F. Alternating Field Demagnetization, Single-Domain-like Memory, and
572 the Lowrie-Fuller Test of Multidomain Magnetite Grains (0.6-356 Mm): AF DEMAGNETIZING
573 MULTIDOMAIN MAGNETITE. J Geophys Res 2004;109(B7); doi: 10.1029/2004JB003006.

574 Dvorkin AY and Steinberger EH. MODELING THE ALTITUDE EFFECT ON SOLAR UV RADIATION. Solar
575 Energy 1999;65(3):181–187; doi: 10.1016/S0038-092X(98)00126-1.

576 Greczynski G and Hultman L. X-Ray Photoelectron Spectroscopy: Towards Reliable Binding Energy
577 Referencing. Progress in Materials Science 2020;107:100591; doi: 10.1016/j.pmatsci.2019.100591.

578 Hansel CM, Zeiner CA, Santelli CM, et al. Mn(II) Oxidation by an Ascomycete Fungus Is Linked to
579 Superoxide Production during Asexual Reproduction. Proceedings of the National Academy of
580 Sciences 2012;109(31):12621–12625; doi: 10.1073/pnas.1203885109.

581 Herkenhoff KE, Golombek MP, Guinness EA, et al. In Situ Observations of the Physical Properties of
582 the Martian Surface. In: The Martian Surface: Composition, Mineralogy and Physical Properties. (Bell
583 J. ed). Cambridge Planetary Science Cambridge University Press: Cambridge; 2008; pp. 451–467; doi:
584 10.1017/CBO9780511536076.021.

585 Hipkin VJ, Voytek MA, Meyer MA, et al. Analogue Sites for Mars Missions: NASA's Mars Science
586 Laboratory and beyond – Overview of an International Workshop Held at The Woodlands, Texas, on
587 March 5–6, 2011. Icarus 2013;224(2):261–267; doi: 10.1016/j.icarus.2013.02.021.

588 Ilton ES, Post JE, Heaney PJ, et al. XPS Determination of Mn Oxidation States in Mn (Hydr)Oxides.
589 Applied Surface Science 2016;366:475–485; doi: 10.1016/j.apsusc.2015.12.159.

590 Jiang Z, Liu Q, Roberts AP, et al. The Magnetic and Color Reflectance Properties of Hematite: From
591 Earth to Mars. Reviews of Geophysics 2022;60(1); doi: 10.1029/2020RG000698.

592 John RE, Chandran A, Thomas M, et al. Surface-Defect Induced Modifications in the Optical
593 Properties of α-MnO2 Nanorods. Applied Surface Science 2016;367:43–51; doi:
594 10.1016/j.apsusc.2016.01.153.

595 Juyal N. Ladakh: The High-Altitude Indian Cold Desert. In: Landscapes and Landforms of India. (Kale
596 VS. ed). World Geomorphological Landscapes Springer Netherlands: Dordrecht; 2014; pp. 115–124;
597 doi: 10.1007/978-94-017-8029-2_10.

598 Kabary H, Eida M, Attia M, et al. Magnetotactic Characterization and Environmental Application P.
599 Aeruginosa Kb1 Isolate. ARRB 2017;20(1):1–10; doi: 10.9734/ARRB/2017/37737.

600 Keim CN, Abreu F, Lins U, et al. Cell Organization and Ultrastructure of a Magnetotactic Multicellular
601 Organism. Journal of Structural Biology 2004;145(3):254–262; doi: 10.1016/j.jsb.2003.10.022.

602 Krinsley D, Dorn RI and DiGregorio B. Astrobiological Implications of Rock Varnish in Tibet.
603 Astrobiology 2009;9(6):551–562; doi: 10.1089/ast.2008.0238.

604 Kuhlman KR, Fusco WG, Duc MTL, et al. Diversity of Microorganisms within Rock Varnish in the
605 Whipple Mountains, California. Applied and Environmental Microbiology 2006; doi:
606 10.1128/AEM.72.2.1708-1715.2006.

607 Kwon KD, Refson K and Sposito G. Surface Complexation of Pb(II) by Hexagonal Birnessite
608 Nanoparticles. Geochimica et Cosmochimica Acta 2010;74(23):6731–6740; doi:
609 10.1016/j.gca.2010.09.002.

610 Lanza NL, Fischer WW, Wiens RC, et al. High Manganese Concentrations in Rocks at Gale Crater,
611 Mars. Geophysical Research Letters 2014a;41(16):5755–5763; doi: 10.1002/2014GL060329.

612 Lanza NL, Fischer WW, Wiens RC, et al. High Manganese Concentrations in Rocks at Gale Crater,
613 Mars. Geophysical Research Letters 2014b;41(16):5755–5763; doi: 10.1002/2014GL060329.

614 Li J, Liu P, Menguy N, et al. Intracellular Silicification by Early-Branching Magnetotactic Bacteria.
615 Science Advances 2022;8(19):eabn6045; doi: 10.1126/sciadv.abn6045.

616 Ling FT, Post JE, Heaney PJ, et al. A Multi-Method Characterization of Natural Terrestrial Birnessites.
617 American Mineralogist 2020;105(6):833–847; doi: 10.2138/am-2020-7303.

618 Liu Q, Roberts AP, Larrasoaña JC, et al. Environmental Magnetism: Principles and Applications. Rev
619 Geophys 2012;50(4):RG4002; doi: 10.1029/2012RG000393.

620 Liu T and Broecker WS. How Fast Does Rock Varnish Grow? Geology 2000;28(2):183–186; doi:
621 10.1130/0091-7613(2000)28<183:HFDRVG>2.0.CO;2.

622 Liu Y, Fischer WW, Ma C, et al. Manganese Oxides in Martian Meteorites Northwest Africa (NWA)
623 7034 and 7533. Icarus 2021;364:114471; doi: 10.1016/j.icarus.2021.114471.

624 Liu Y, Li GR, Guo FF, et al. Large-Scale Production of Magnetosomes by Chemostat Culture of
625 Magnetospirillum Gryphiswaldense at High Cell Density. Microbial Cell Factories 2010;9(1):99; doi:
626 10.1186/1475-2859-9-99.

627 Lowenstam HA and Weiner S. Biomineralization Processes. In: On Biomineralization Oxford
628 University Press; 1989; doi: 10.1093/oso/9780195049770.003.0005.

629 Luo S, Qin J, Wu Y, et al. Tetracycline Adsorption on Magnetic Sludge Biochar: Size Effect of the
630 Fe3O4 Nanoparticles. Royal Society Open Science 2022;9(1):210805; doi: 10.1098/rsos.210805.

631 Magnuson JK and Lasure LL. Organic Acid Production by Filamentous Fungi. In: Advances in Fungal
632 Biotechnology for Industry, Agriculture, and Medicine. (Tkacz JS and Lange L. eds) Springer US:
633 Boston, MA; 2004; pp. 307–340; doi: 10.1007/978-1-4419-8859-1_12.

Mancinelli RL, J.L. Bishop, and De S. MAGNETITE IN DESERT VARNISH AND APPLICATIONS TO ROCK VARNISH ON MARS. Lunar and Planetary Science XXXIII (2002): LSunar and Planetary Institute, Houston.; 2002.

Mills P and Sullivan JL. A Study of the Core Level Electrons in Iron and Its Three Oxides by Means of X-Ray Photoelectron Spectroscopy. J Phys D: Appl Phys 1983;16(5):723–732; doi: 10.1088/0022-3727/16/5/005.

Mira N and Teixeira M. Microbial Mechanisms of Tolerance to Weak Acid Stress. Frontiers in Microbiology 2013;4.

Muhler M, Schlögl R and Ertl G. The Nature of the Iron Oxide-Based Catalyst for Dehydrogenation of Ethylbenzene to Styrene 2. Surface Chemistry of the Active Phase. Journal of Catalysis 1992;138(2):413–444; doi: 10.1016/0021-9517(92)90295-S.

Nesbitt HW and Banerjee D. Interpretation of XPS Mn(2p) Spectra of Mn Oxyhydroxides and Constraints on the Mechanism of MnO2 Precipitation. American Mineralogist 1998;83(3–4):305–315; doi: 10.2138/am-1998-3-414.

Norberg and Hodge. Ladakh: Development without Destruction. In: In: J.S. Lall (Ed.), The Himalaya: Aspects of Change Delhi: Oxford University; 1995; pp. 142-148.

Pandey S, Clarke J, Nema P, et al. Ladakh: Diverse, High-Altitude Extreme Environments for off-Earth Analogue and Astrobiology Research. International Journal of Astrobiology 2020;19(1):78–98; doi: 10.1017/S1473550419000119.

Perry RS and Adams JB. Desert Varnish: Evidence for Cyclic Deposition of Manganese. Nature 1978;276(5687):489–491; doi: 10.1038/276489a0.

Perry RS and Hartmann WK. Mars Primordial Crust: Unique Sites for Investigating Proto-Biologic Properties. Orig Life Evol Biosph 2006;36(5):533–540; doi: 10.1007/s11084-006-9037-2.

Perry RS and Sephton MA. Desert Varnish: An Environmental Recorder for Mars. Astronomy & Geophysics 2006;47(4):4.34-4.35; doi: 10.1111/j.1468-4004.2006.47434.x.

Phartiyal B, Singh R, Joshi P, et al. Late-Holocene Climatic Record from a Glacial Lake in Ladakh Range, Trans-Himalaya, India. The Holocene 2020;30(7):1029–1042; doi: 10.1177/0959683620908660.

Phartiyal B, Singh R, Nag D, et al. Reconstructing Climate Variability during the Last Four Millennia from Trans-Himalaya (Ladakh-Karakoram, India) Using Multiple Proxies. Palaeogeography, Palaeoclimatology, Palaeoecology 2021;562:110142; doi: 10.1016/j.palaeo.2020.110142.

Pósfai M and Dunin-Borkowski RE. Sulfides in Biosystems. Reviews in Mineralogy and Geochemistry 2006;61(1):679–714; doi: 10.2138/rmg.2006.61.13.

Potter RM and Rossman GR. Desert Varnish: The Importance of Clay Minerals. Science 1977; doi: 10.1126/science.196.4297.1446.

Potter RM and Rossman GR. The Manganese- and Iron-Oxide Mineralogy of Desert Varnish. Chemical Geology 1979;25(1):79–94; doi: 10.1016/0009-2541(79)90085-8.

671 Preston LJ and Dartnell LR. Planetary Habitability: Lessons Learned from Terrestrial Analogues.
672 International Journal of Astrobiology 2014;13(1):81–98; doi: 10.1017/S1473550413000396.

673 Rabchinskii MK, Dideikin AT, Kirilenko DA, et al. Facile Reduction of Graphene Oxide Suspensions and
674 Films Using Glass Wafers. Sci Rep 2018;8(1):14154; doi: 10.1038/s41598-018-32488-x.

675 Rochette P, Gattacceca J, Chevrier V, et al. Magnetism, Iron Minerals, and Life on Mars. Astrobiology
676 2006;6(3):423–436; doi: 10.1089/ast.2006.6.423.

677 Rouxhet PG and Genet MJ. XPS Analysis of Bio-Organic Systems. Surface and Interface Analysis
678 2011;43(12):1453–1470; doi: 10.1002/sia.3831.

679 Sangode SJ, Rawat S, Meshram DC, et al. Integrated Mineral Magnetic and Lithologic Studies to
680 Delineate Dynamic Modes of Depositional Conditions in the Leh Valley Basin, Ladakh Himalaya,
681 India. Geological Society of India 2013;82(2):107–120.

682 Santelli CM, Webb SM, Dohnalkova AC, et al. Diversity of Mn Oxides Produced by Mn(II)-Oxidizing
683 Fungi. Geochimica et Cosmochimica Acta 2011;75(10):2762–2776; doi: 10.1016/j.gca.2011.02.022.

684 Schmidt S and Nüsser M. Changes of High Altitude Glaciers in the Trans-Himalaya of Ladakh over the
685 Past Five Decades (1969–2016). Geosciences 2017;7(2):27; doi: 10.3390/geosciences7020027.

686 Sharma A and Phartiyal B. Late Quaternary Palaeoclimate and Contemporary Moisture Source to
687 Extreme NW India: A Review on Present Understanding and Future Perspectives. Frontiers in Earth
688 Science 2018;6.

689 Singh S, Sahoo RK, Shinde NM, et al. Synthesis of Bi2O3-MnO2 Nanocomposite Electrode for Wide-
690 Potential Window High Performance Supercapacitor. Energies 2019;12(17):3320; doi:
691 10.3390/en12173320.

692 Stacey FD. Theory of the Magnetic Properties of Igneous Rocks in Alternating Fields. The
693 Philosophical Magazine: A Journal of Theoretical Experimental and Applied Physics 1961;6(70):1241–
694 1260; doi: 10.1080/14786436108243374.

695 Sun X, Duffort V, Mehdi BL, et al. Investigation of the Mechanism of Mg Insertion in Birnessite in
696 Nonaqueous and Aqueous Rechargeable Mg-Ion Batteries. Chem Mater 2016;28(2):534–542; doi:
697 10.1021/acs.chemmater.5b03983.

698 Tan J and Sephton MA. Organic Records of Early Life on Mars: The Role of Iron, Burial, and Kinetics
699 on Preservation. Astrobiology 2020;20(1):53–72; doi: 10.1089/ast.2019.2046.

700 Toner B, Manceau A, Webb SM, et al. Zinc Sorption to Biogenic Hexagonal-Birnessite Particles within
701 a Hydrated Bacterial Biofilm. Geochimica et Cosmochimica Acta 2006;70(1):27–43; doi:
702 10.1016/j.gca.2005.08.029.

703 Villalobos M, Lanson B, Manceau A, et al. Structural Model for the Biogenic Mn Oxide Produced by
704 Pseudomonas Putida. American Mineralogist 2006;91(4):489–502; doi: 10.2138/am.2006.1925.

705 Villalobos M, Toner B, Bargar J, et al. Characterization of the Manganese Oxide Produced by
706 Pseudomonas Putida Strain MnB1. Geochimica et Cosmochimica Acta 2003;67(14):2649–2662; doi:
707 10.1016/S0016-7037(03)00217-5.

708 Walden J. Sample Collection and Preparation. In: Walden, J., Oldfield, F. and Smith, J.P. (Eds) 1998
709 Environmental Magnetism: A Practical Guide. In: 1998 Environmental Magnetism: A Practical Guide
710 Technical Guide Series, No 6,. (Walden J, Oldfield F, and Smith J. eds) Quaternary Research
711 Association; 1999; pp. 26–34.

712 Yamashita T and Hayes P. Analysis of XPS Spectra of Fe2+ and Fe3+ Ions in Oxide Materials. Applied
713 Surface Science 2008;254(8):2441–2449; doi: 10.1016/j.apsusc.2007.09.063.

714 Yang T, Liu Q, Li H, et al. Anthropogenic Magnetic Particles and Heavy Metals in the Road Dust:
715 Magnetic Identification and Its Implications. Atmospheric Environment 2010;44(9):1175–1185; doi:
716 10.1016/j.atmosenv.2009.12.028.

717 Yun S, Hwang H, Hwang G, et al. Super-Hydration and Reduction of Manganese Oxide Minerals at
718 Shallow Terrestrial Depths. Nat Commun 2022;13(1):1942; doi: 10.1038/s41467-022-29328-y.

719

720

721

722

723

724

725

726

727

728

729

730

731

732

733

734

735

736

737

738

739

740

Supplementary Information

Ladakh's Rock Varnish: A potential Geomaterial for astrobiological studies

Amritpal Singh Chaddha[*a, b], Anupam Sharma[*a], Narendra Kumar Singh[b], Sheikh Nawaz Ali[a], P.K. Das[a], S.K. Pandey[a], Binita Phartiyal[a], Subodh Kumar[a]

[a]Birbal Sahni Institute of Palaeosciences, 53 University Road, Lucknow-226007, India

[b]Department of Chemistry, Faculty of Science, University of Lucknow, Lucknow-226007, India

[*]E-mail: anupam110367@gmail.com; amrit.chemsingh@gmail.com

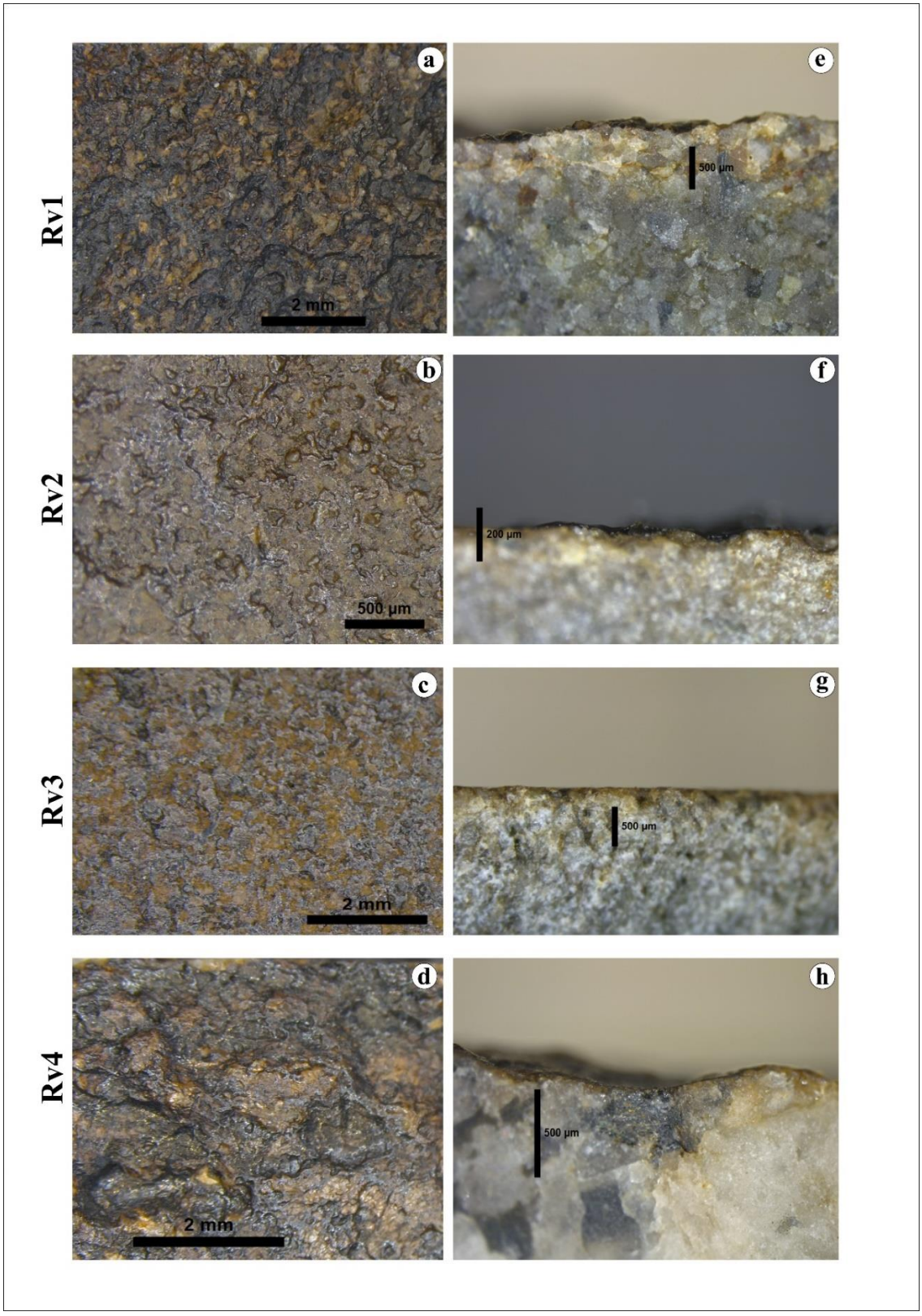

Fig.S1 (a-d) Optical microscopic image of surface of varnish Layer; (e-h) Side view of the cross- section of sample showing host rock (substrate) on which varnish layer was deposited.

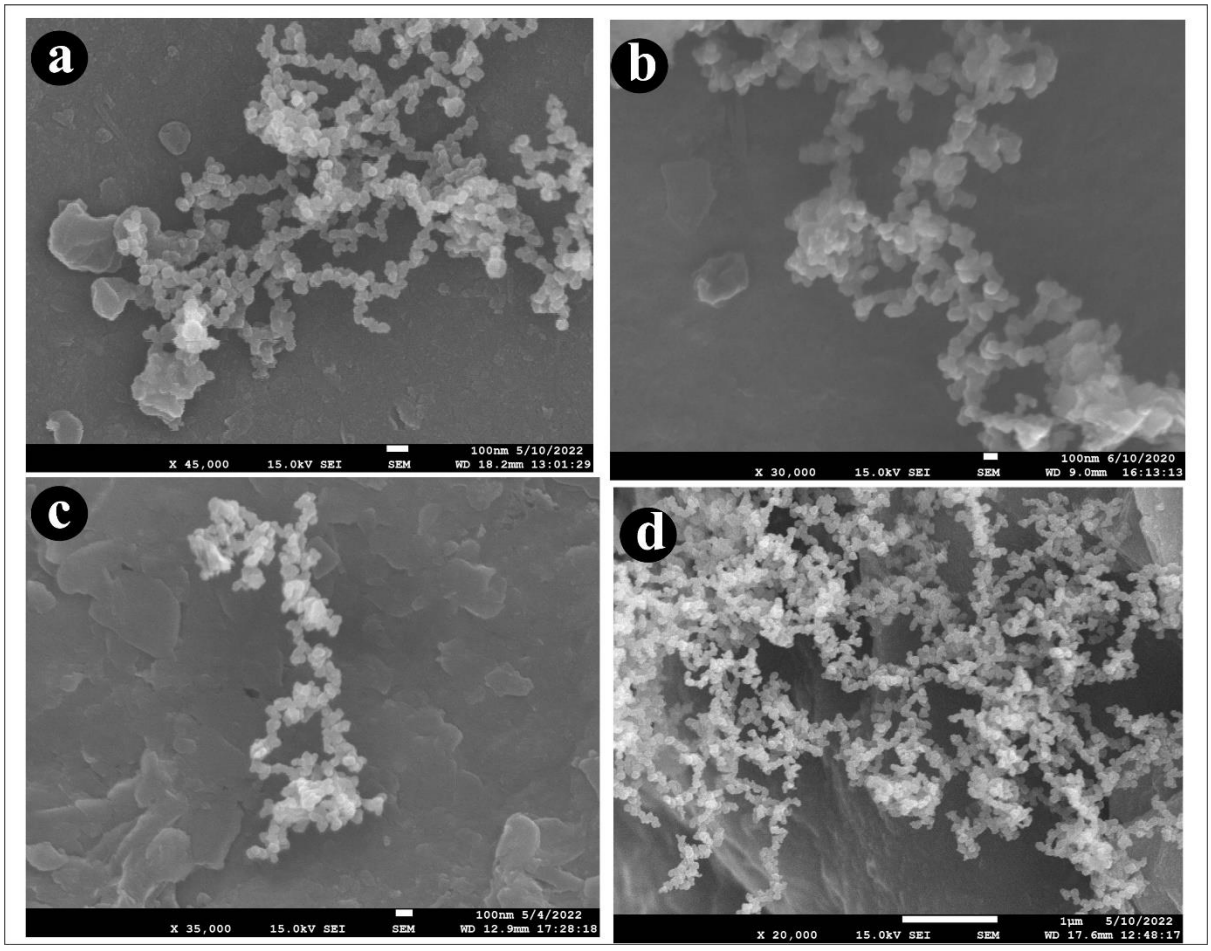

Fig.S2(a-d) chain like morphology of magnetosomes on various varnish samples.

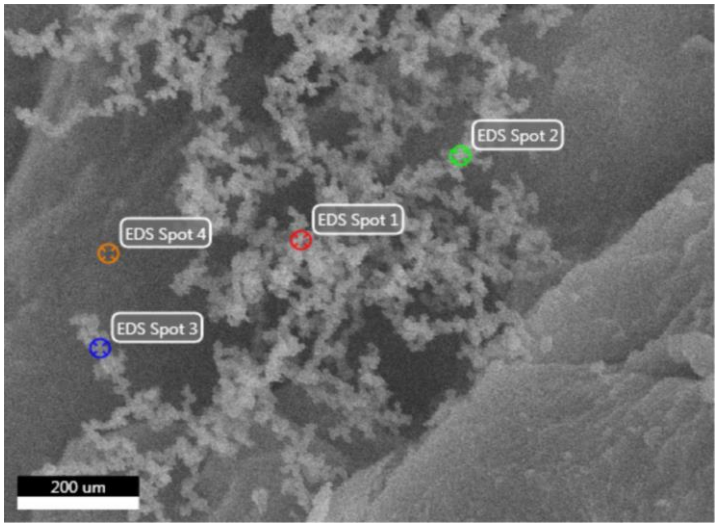

Fig.S3 Multi-spot EDS elemental analysis of the chain like clusters with chemical composition of each spot 1,2,3,4 is given below.

EDS-SPOT-1

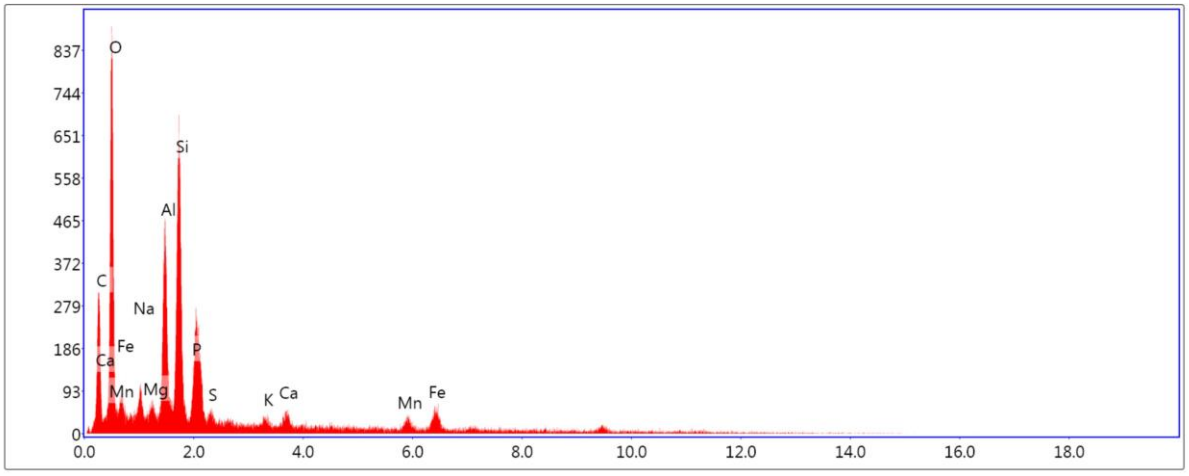

EDS-SPOT-2

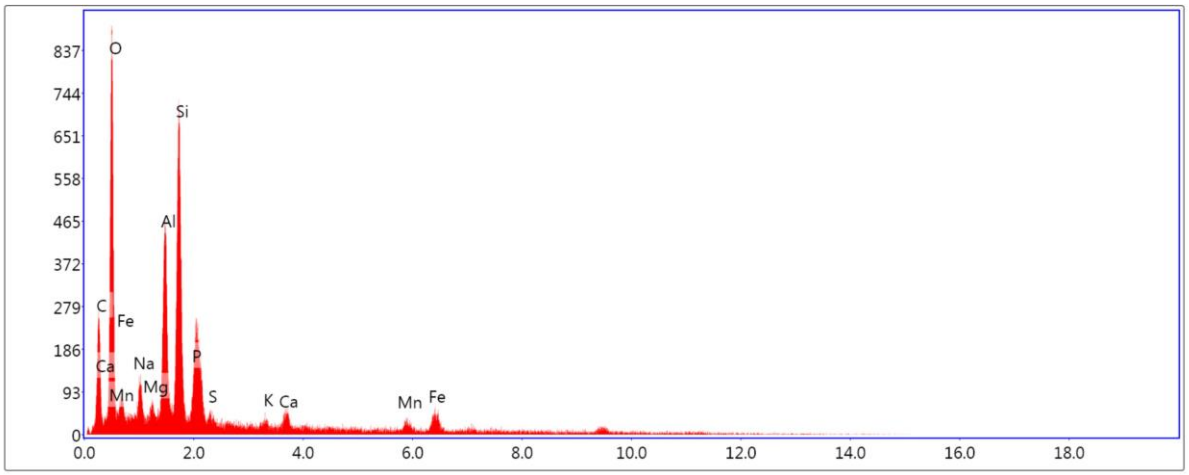

Lsec: 50.0 0 Cnts 0.000 keV Det: Octane Plus Det

EDS-SPOT-3

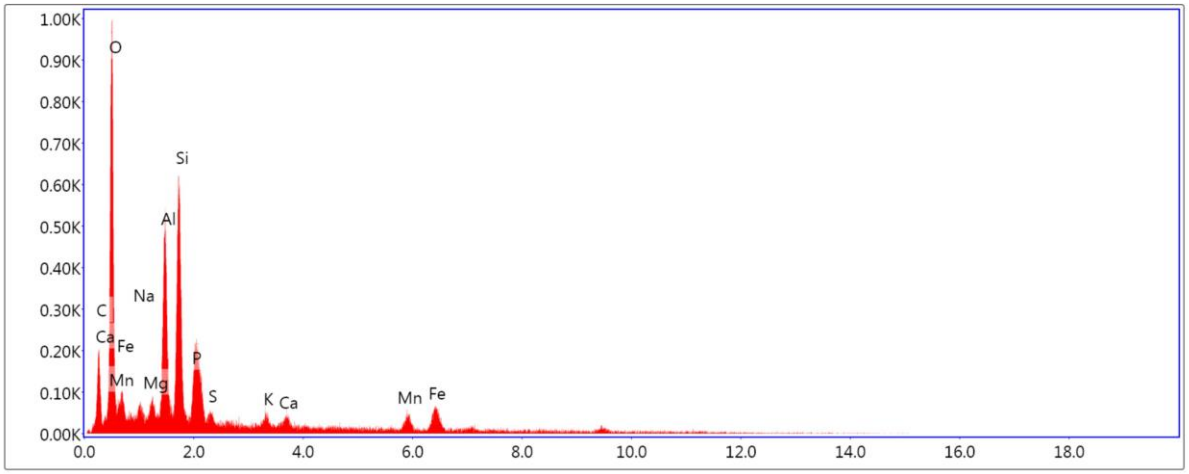

Lsec: 50.0 0 Cnts 0.000 keV Det: Octane Plus Det

EDS-SPOT-4

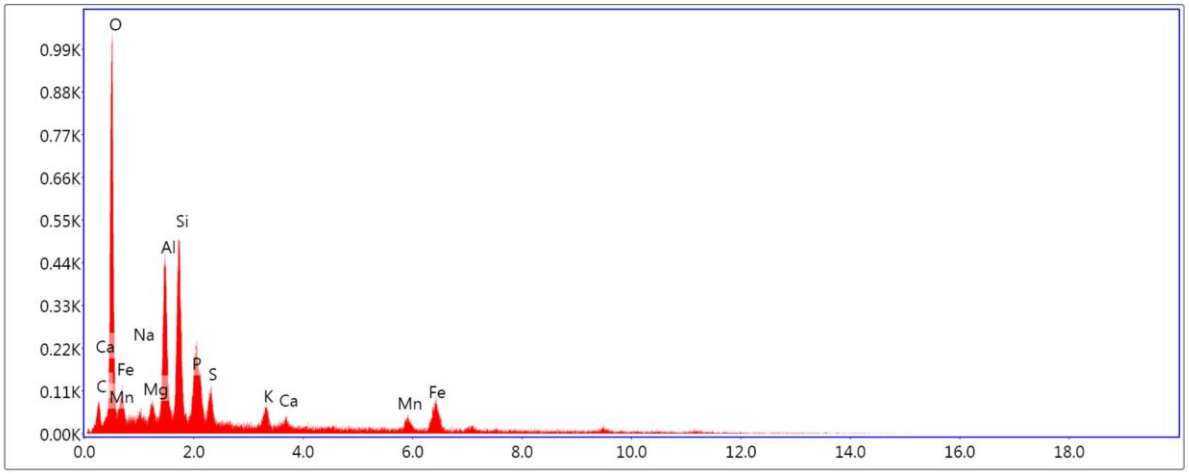

Lsec: 50.0 0 Cnts 0.000 keV Det: Octane Plus Det

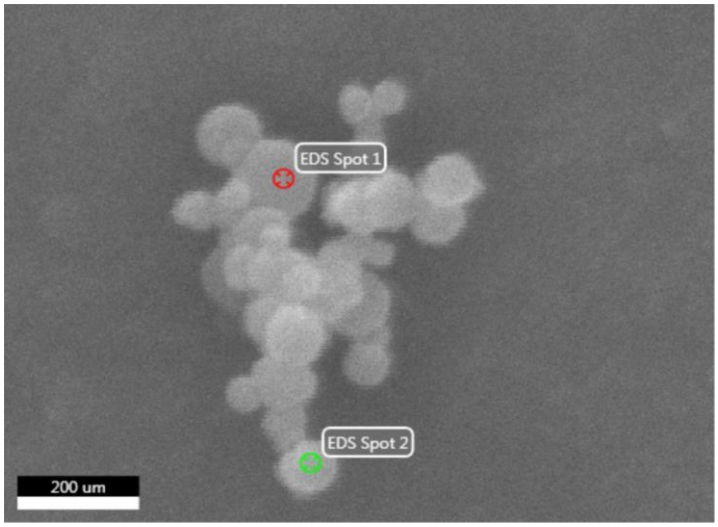

Fig.S4 Multi-spot high resolution EDS elemental analysis of the chain like clusters with chemical composition of each spot 1,2 given below.

EDS-SPOT-1

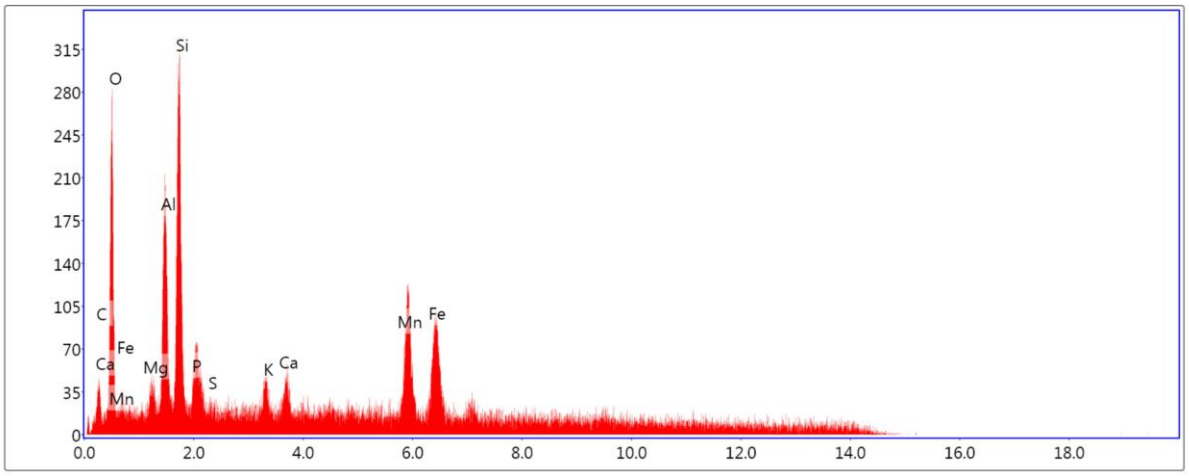

Lsec: 50.0 0 Cnts 0.000 keV Det: Octane Plus Det

EDS-SPOT-2

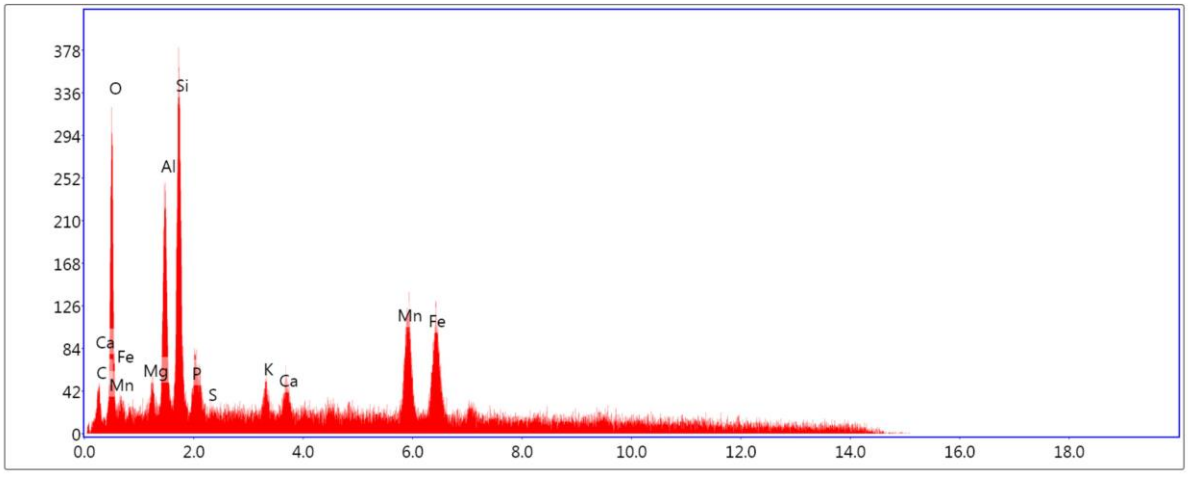

Lsec: 50.0 0 Cnts 0.000 keV Det: Octane Plus Det

HS.1 Detailed petrological investigation of the host rock.

Texturally, first two sections of the clastic deposit of the Indus Molasses are coarser (a-d) than the third one (e-f). The thin sections representing the Indus Molasses comprises mainly anhedral to subhedral quartz grains (70%). Quartz grains are angular and poorly sorted associated with feldspar and lithic fragment with clay fine matrix probably close to the greywacke (a variety of sandstone). Few quartz grains are prismatic, but most grains are anhedral, whereas some are tabular and irregular in shape (Fig.7e-f). No preferred orientation and long contact seen in prismatic and tabular quartz grains whereas, concave and convex contact seen (Fig.7 a-f). Diagenetic silica overgrowth has not been noticed on the sub-rounded quartz grains. Monocrystalline quartz grains dominate the assemblage (75%) with subordinate sizable population of polycrystalline grains (25%). Very few small squares to almost rectangle shape shaped opaque magnetite/ibm (iron bearing mineral) inclusions are noticed in samples represented by the India Molasses (Fig.7 c-d). Feldspar constitutes about 10% of the entire grain population (Fig.7 e-f). Na feldspars consist of tabular grains of plagioclase with characteristic twinning, triclinic shape, with first order grey colour. Lath/flaky shaped mica are constituted of biotite, sericite and muscovite showing no preferred orientation similar to quartz grains. Under polarized light, biotite shows prominent pleochroism from light brown to dark brown. Muscovite shows second order interference colour under crossed polars. Rarely, iron bearing matrix is present in between quartz grains which are derived from alteration of biotite or iron bearing mineral such as magnetite (Fig.7 a-b). Thin section represented by the very coarse grained Ladakh Batholith i.e., Fig g-h shows heavy amount of magnetite/ibm associated with other essential (quartz and feldspar) and subordinate minerals (mica bearing mineral such as muscovite). Quartz grains are subhedral to euhedral in shape with concave and convex contact. No long contact between the quartz grain seen (Fig. g-h). Quartz inclusions can be seen within the magnetite/ibm.

Table.1 Details of various magnetic parameters with S-ratio values.

Sample	Mass (gm)	χ_{lf} ($10^{-8}m^3kg^{-1}$)	ARM ($10^{-5}Am^2kg^{-1}$)	SIRM ($10^{-5}Am^2kg^{-1}$)	Soft IRM ($10^{-5}Am^2kg^{-1}$)	S-Ratio
1v	0.4	238.1	6.71	1045.0	754.5	0.98
2v	0.38	496.0	13.01	2018.4	1313.2	0.99
3v	0.38	819.0	17.56	2871.1	1842.1	0.98
4v	0.5	1068.2	22.46	5760.0	5054.0	0.99
1H	7.59	28.0	2.47	967.1	715.9	1.00
2H	7.85	11.3	0.70	51.2	26.8	0.81
3H	6.48	4.6	0.17	27.9	13.3	0.97
4H	7.1	616.2	29.10	12436.6	8985.9	1.00

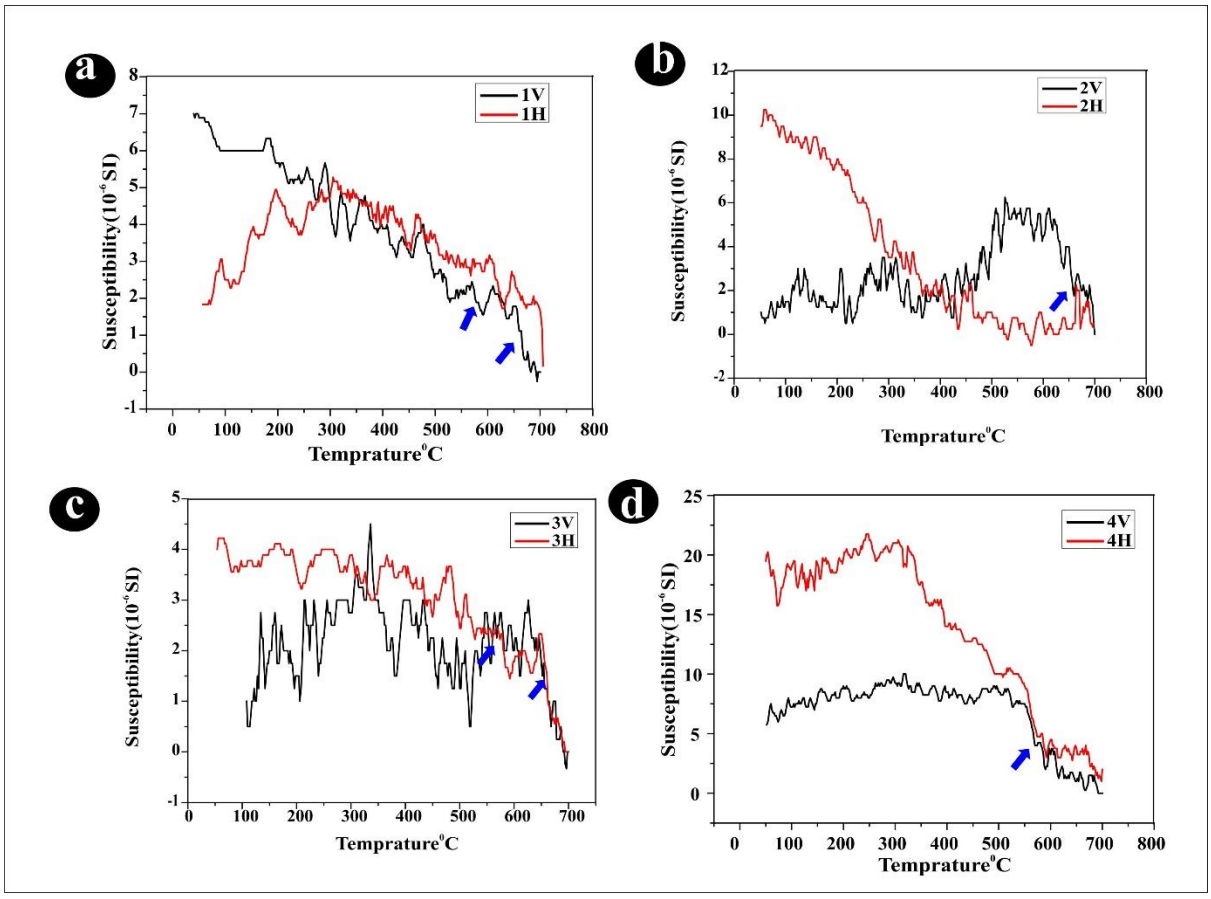

Fig.S5 (a-d) Temperature variation of magnetic susceptibility(χ-T) scans of the investigated samples displaying magnetite and haematite shown in blue arrows.